Journal of Drug Delivery Science and Technology 117 (2026) 108018

Contents lists available at ScienceDirect

Journal of Drug Delivery Science and Technology

journal homepage: www.elsevier.com/locate/jddst

Liposomal co-formulation of Azure A and rose bengal decyl ester as a multi-cellular target approach for photodynamic therapy of colorectal cancer

Ana Claudia Pedrozo da Silva [a,b,*], Camila Fabiano de Freitas [c], Italo Rodrigo Calori [d], Antonio Claudio Tedesco [e], Amanda Gratão Silvestrin [f], Leandro Herculano da Silva [g,h], Maria Ida Bonini Ravanelli Speziali [f], Noboru Hioka [a], André Luiz Tessaro [b,**]

[a] Department of Chemistry, State University of Maringá, Maringá, Paraná, Brazil
[b] Research Group of Active Materials, Federal Technology University, Apucarana, Paraná, Brazil
[c] Department of Chemistry, Federal University of Santa Catarina, Florianópolis, Santa Catarina, Brazil
[d] Pharmaceutical Engineering and 3D Printing (PharmE3D) Labs, Department of Pharmaceutics and Drug Delivery, School of Pharmacy, The University of Mississippi, University, United States
[e] Department of Chemistry, Center of Nanotechnology and Tissue Engineering- Photobiology and Photomedicine Research Group, Faculty of Philosophy, Sciences and Letters of Ribeirão Preto, University of São Paulo, Ribeirão Preto, São Paulo, Brazil
[f] Department of Physiological Sciences, State University of Maringá, Maringá, Paraná, Brazil
[g] Departamento de Física, Universidade Tecnológica Federal do Paraná, Campus Medianeira. Av. Brazil, 4232, CEP 85.722-332, Medianeira, Paraná, Brazil
[h] CIMO, LA SusTEC, Instituto Politécnico de Bragança, Campus de Santa Apolónia, 5300-253, Bragança, Portugal

ARTICLE INFO

Keywords:
Phenothiazine
Xanthene
Photodynamic therapy
Combined system
Cancer

ABSTRACT

Multidrug systems offer a promising strategy to improve the efficacy of anticancer treatments, reduce therapeutic doses, and attenuate side effects. In this study, the photosensitizers Azure A (AA) and rose bengal decyl ester (RBDEC) were co-encapsulated in hybrid DPPC/F127 liposomes to target multiple cellular sites. The combined system yielded small unilamellar vesicles (SUVs) with a polydispersity index suitable for biological applications and a zeta potential of +10.57 mV. The encapsulation efficiency of AA and RBDEC is 60.3 and 98.5 %, respectively. In the colorectal adenocarcinoma Caco-2 cells line, photosensitizers showed distinct cellular localization, with RBDEC most targeting the nuclear region and AA the cytoplasm confirmed by confocal microscopy. According to the Chou–Talalay method for drug combinations, the equimolar and lower concentrations (2.5×10^{-6} mol L^{-1} each) exhibited an additive effect, suggesting that even lower concentrations could achieve synergism. The findings indicate that this system exhibits considerable promise, as the combination of drugs facilitates action at multiple sites, thereby increasing the likelihood of cell death. In addition, the system demonstrated greater efficiency at lower concentrations, reducing adverse effects and directing future studies.

1. Introduction

Photodynamic therapy (PDT) has been the subject of extensive clinical research to treat various oncological and non-oncological diseases for several decades. PDT is a minimally invasive and minimally toxic treatment technique that is effective in several types of cancer [1, 2]. However, despite the considerable progress achieved, it remains imperative that studies on new photosensitizers and formulations advance with even more intelligent, effective, and accessible systems, particularly in cancer treatment.

PDT is a treatment technique that utilizes light as a trigger for the activation of a photosensitizer in the presence of molecular oxygen, leading to the generation of singlet oxygen and other reactive oxygen species [3]. Given its targeted nature, this technique has emerged as a promising modality in cancer treatment, which minimizes adverse effects and enhances prognosis. PDT can be utilized as a single modality or in combination with other therapeutic approaches [4]. Its mechanism of action involves the occurrence of cellular data in the precise subcellular

* Corresponding author. Marcílio Dias, 635 CEP 86812-460, Apucarana, PR, Brazil.
** Corresponding author. Marcílio Dias, 635 CEP 86812-460, Apucarana, PR, Brazil.
E-mail addresses: anacsilva@utfpr.edu.br (A.C. Pedrozo da Silva), andretessaro@utfpr.edu.br (A.L. Tessaro).

https://doi.org/10.1016/j.jddst.2026.108018
Received 30 June 2025; Received in revised form 11 January 2026; Accepted 13 January 2026
Available online 14 January 2026

location of the PS, a consequence of the short radius of action of singlet oxygen. Consequently, the intracellular distribution of the photosensitizer is a key factor in the cellular responses induced by light. This subcellular localization is primarily dictated by the chemical properties of the molecule and can be strategically modulated to enhance selectivity and therapeutic efficacy [5].

Numerous studies have demonstrated the advantages of incorporating multiple drugs into a single formulation for anticancer therapy. A notable example is CPX-351® (VYXEOS), a liposomal formulation that co-encapsulates cytarabine and daunorubicin at a fixed synergistic ratio. This combination demonstrated superior efficacy and reduced toxicity compared to the conventional 7 + 3 regimen, leading to FDA approval in 2017 for adult patients with high-risk acute myeloid leukemia and subsequent expansion of the indication in 2021 to include pediatric patients aged one year and older [6,7]. The relevance of dual-photosensitizer system lies in the attempt to overcome the limitations associated with monotherapy. Using two PSs can enable a synergistic or additive effect, thereby addressing the shortcomings of a single-photosensitizer approach. Such strategies can enhance therapeutic efficacy, reduce dark cytotoxicity by reducing the total concentration, and potentially minimize adverse effects. Moreover, dual-PS therapy may offer the benefit of multi-targeting therapy, contributing to a more comprehensive therapeutic outcome [8]. Some studies have also reported the use of combinations of photosensitizers, including phthalocyanine/porphyrin [9,10], hypericin/chlorin [11], hypericin/ALA [12], and two different cyanine dyes which operates via type I and II mechanisms [13]. These studies underscore the importance of the cellular location of photosensitizers for effective singlet oxygen ($^1O_2$) attack, given the short half-life of this cytotoxic species. Moreover, the co-formulation of the "two bullets" in liposomal systems may represent an elegant and effective strategy, as liposomes allow for the incorporation of molecules with different hydrophobicities while aligning the pharmacokinetic profiles of the drugs [6].

In our previous study, we demonstrated that small unilamellar lipid-polymer hybrid liposomes could be prepared rapidly and cost-effectively to stabilize xanthenes, such as Rose Bengal and hydrophobic derivatives [14]. In this context, the objective of this study was to co-encapsulate two photosensitizers, the hydrophilic photosensitizer Azure A (AA) (log P = 0.08) [15] and the hydrophobic rose bengal decyl ester (RBDEC) (log P = 1.98) [16], in hybrid DPPC/F127 liposomes. This innovative approach seeks to leverage the distinct properties of each photosensitizer, seeking to act simultaneously on multiple cellular sites to increase photodynamic efficiency. The chemical structures of these compounds are depicted in Fig. 1.

2. Experimental section

2.1. Materials

The 1,2-dipalmitoyl-sn-glycero-3-phosphatidylcholine was purchased from Avanti Polar Lipids (Alabama, USA). Pluronic® F127 (M = 12500 g mol^{-1}), Rose Bengal disodium salt, Erythrosine B, Azure A chloride, 1-bromodecane, trehalose (Tre), 1,6-Diphenyl-1,3,5-hexatriene (DPH), 9,10-anthracenediyl-bis(methylene)dimalonic acid (ABDA), 3-(4,5-dimethylthiazol-2-yl)-2,5-diphenyl tetrazolium bromide (MTT), DMEM (Dulbecco's Modified Eagle Medium) culture medium and Microcon-10kDa centrifugal filters were purchased from Sigma-Aldrich/Merck. The water used was double-distilled. The RBDEC stock (1.5×10^{-3} mol L^{-1}) was prepared in dimethyl sulfoxide (DMSO), and the Azure A stock (1.5×10^{-3} mol L^{-1}) was prepared in ethanol. Both were stored under refrigeration, protected from light and periodically standardized by UV–Vis absorption. All solvents employed were of analytical grade and were used without further purification.

2.2. Preparation and characterization of isolated and combined dye formulations

DPPC/F127 liposomes were prepared by thin film methodology, as previously reported by Freitas et al. [17]. The final concentration of DPPC was fixed at 1.5×10^{-3} mol L^{-1} and the F127 concentration at 2.0×10^{-5} mol L^{-1} (0.025 % m/V). The esterification of RB for the synthesis of RBDEC was previously described by Pereira et al. [16] and the synthesis was confirmed by H^1-NMR (500 MHz). The mean hydrodynamic diameter (D_H), polydispersity index (PI), and zeta potential (ζ) were obtained via dynamic light scattering (DLS) using the Litesizer-500 (Anton Paar, Graz, Austria). After incorporating the PS, UV–Vis absorbance and fluorescence emission spectroscopic analyses were conducted using a Cary 60 UV–Vis spectrophotometer and a Cary Eclipse spectrofluorimeter (Agilent Technologies, USA). For the fluorescence emission of RBDEC, λ_{exc} = 520 nm was used and for AA λ_{exc} = 570 nm. For the combined system, λ_{exc} will be determined during the study. The morphology of the vesicles was evaluated by transmission electron microscopy (TEM) using a JEM-2100 transmission electron microscope (JEOL, Japan) operated at an acceleration voltage of 100 kV. The samples were prepared using trehalose as cryoprotectant (3.0×10^{-4} mol L^{-1}). These samples were diluted 100x, and a drop was placed on formvar-covered copper grids. The grids were quickly submerged in liquid nitrogen and lyophilized for 30 min to improve image resolution [18].

The samples produced in this study are designated as DPPC/F127/RBDEC, DPPC/F127/AA, and DPPC/F127/RBDEC/AA, wherein both

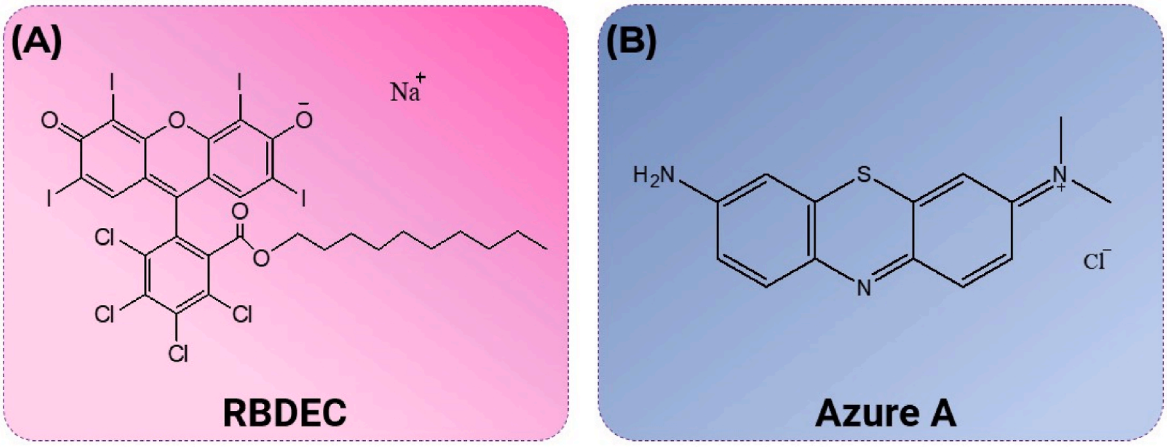

Fig. 1. Chemical structure of (A) RBDEC and (B) Azure A.

PSs were encapsulated in a 1:1 ratio. The concentration of PS in the isolated systems was 5.0×10^{-6} mol L^{-1}. In the combined system, the concentration of each PS was maintained at 5.0×10^{-6} mol L^{-1}, resulting in a total [PS] of 1.0×10^{-5} mol L^{-1}. Two incorporation strategies were investigated: (i) dual passive loading, in which both PSs (AA and RBDEC) were simultaneously added to the aqueous hydration medium; and (ii) combined active–passive loading, in which AA was incorporated into the organic phase together with the lipids prior to solvent evaporation (active loading), and RBDEC was added during hydration (passive loading). To ascertain the degree of synergism exhibited by the mixed system, variations in dye concentration were employed in the phototoxicity assay. The results of this experiment will be presented in the following section.

The apparent molar absorptivity (ε_{app}) of RBDEC and AA encapsulated in the liposomal vesicles was determined by Lambert-Beer law. The encapsulation efficiency (EE%) was quantified by centrifugation through Microcon-10kDa centrifugal filters. The formulations were centrifuged at 13,000 rpm for 30 min and free PSs were quantified by fluorescence emission. The results were obtained according to Equation (1) and are presented as the mean of three independent measurements (n = 3) ± standard deviation.

$$EE\% = \frac{Incorporated\ PS}{Total\ PS}\ x\ 100 \quad (1)$$

2.3. Interaction and stability studies of formulations

The stability of the formulations was evaluated through the use of UV–Vis electronic absorption spectrophotometry, fluorescence emission spectroscopy, and dynamic light scattering (DLS). Regarding storage stability, the systems were characterized for 60 days, consistently shielded from light, and maintained at room temperature. For determining shelf-life, the samples were subjected to lyophilization and stored at 4 °C for 12 months. The lyophilized samples were comprised of trehalose as a cryoprotectant (3.0×10^{-4} mol L^{-1}). Following this period, the lyophilized formulations were dispersed in ultrapure water and subjected to further characterization. Furthermore, the stability of the formulations was evaluated in response to temperature variations. To this end, 2.0 mL of each sample was subjected to temperatures ranging from 25.0 to 50.0 °C, and the absorption, emission, and hydrodynamic diameter were characterized. In addition, the formulations were evaluated for dilution stability. Dilutions were performed at 10x and 100x concentrations in phosphate buffered saline (PBS).

Encapsulation kinetics evaluates the time required for the PS to enter the vesicle, referred to here as passive encapsulation. To evaluate encapsulation kinetics, a small aliquot of PS stock solution was added to 2.0 mL of liposomal solution ([PS] = 5.0×10^{-6} mol L^{-1}) and emission data acquisition began immediately. Release kinetics experiments were performed using the dialysis method [14]. Each sample was placed in a dialysis bag (MWCO = 3500 Da, Spectra/Por®) and immersed in 100 mL of PBS containing F127 (0.5 % w/v) at either pH 7.4 or pH 6.5. The systems were maintained at 37.0 °C to simulate body temperature. At each time interval, an aliquot was removed, and its fluorescence emission was recorded, followed by replacement with fresh solution to maintain sink conditions. Quantitative analysis of the PS was performed using fluorescence emission measurements and a previously constructed fluorescence calibration curve.

2.4. Estimating the location of photosensitizers in the liposome

Fluorescence quenching of the systems was performed using iodide ion as a water-soluble quencher (KI 1.0 mol L^{-1}). In this experiment, 2.0 mL of the sample was added to a cuvette and successive additions of KI were made to a final volume of 3.0 mL. The dilution factor was corrected so that only the quenching effect could be evaluated. The Stern-Volmer constant (K_{SV}) was then calculated using Equation (2).

$$\frac{F_0}{F} = 1 + K_{SV}[I^-] \quad (2)$$

Where F_0 and F are the fluorescence intensities in the absence and presence of the quencher, respectively, and [I^-]: is the molar concentration of iodide.

For fluorescence resonance energy transfer (FRET) assays, the DPH probe encapsulated in liposomes (1.0×10^{-6} mol L^{-1}, energy donor) was titrated with successive aliquots of PS (energy acceptor). DPH was incorporated into the liposomes by active methodology, i.e. during the formation of the thin film. After each addition of PS, the time necessary for its internalization was waited and then the fluorescence emission spectrum was recorded (λ_{exc} = 360 nm, energy donor). All analyses were performed at 25 °C. The equations used are found in the works of Lakowicz [19] and Silva [14].

2.5. Determination of singlet oxygen quantum yield ($\phi_\Delta^1 O_2$)

The singlet oxygen quantum yield ($\phi_\Delta^1 O_2$) was determined via an indirect method using *9,10-anthracenediyl-bis(methylene)dimalonic acid* (ABDA) as a probe. The experiments were conducted in a quartz cuvette with an optical path length of 1.0 cm, containing an aqueous solution of ABDA (2.0 mL, 6.0×10^{-5} mol L^{-1}) and the sample (5.0×10^{-6} mol L^{-1}). In the case of samples containing liposomes, ABDA was left in contact with the sample in the dark for 1 h before the commencement of illumination. This period is sufficient for the diffusion of ABDA through the lipid bilayer, thereby increasing its proximity to the photosensitizers [14].

In the course of irradiation experiments, the evolution of ABDA photodegradation was evaluated over 360 min using a Cary 60 UV–Vis spectrophotometer (Agilent Technologies, USA) operating in kinetic scanning mode. The illumination was conducted with a cylindrical reactor equipped with a warm white emission LED, situated at a distance of 3.0 cm from the liquid surface, with an irradiance of 32.0 mW cm^{-2}. As the spectrophotometer operates in phase-radiation mode, the incidence of external light does not affect the results, ensuring the reliability of the data. The overlap of the LED emission spectrum and the formulation's absorbance spectra is illustrated in Fig. S1. It is important to highlight that the emission spectrum of the LED does not overlap with the absorption spectrum of ABDA. In other words, the photodynamic effect (light + PS) is responsible for ABDA degradation, not just illumination.

The kinetics of photodegradation were evaluated at λ = 400 nm, and a first-order monoexponential kinetic equation was fitted to the experimental data, thereby obtaining the rate constant of this reaction (k_{ABDA}). The same adjustment was performed on the λ_{max} of absorption of each dye, thus obtaining the photobleaching constant (k_{PB}). A series of equations were required to calculate the singlet oxygen quantum yield, which is detailed and explained in the research of Rabello et al. [20] Rose Bengal in an aqueous medium and xanthene Erythrosine B (ERY) incorporated in DPPC/F127 were compared as a standard. The singlet oxygen quantum yield for the DPPC/F127/ERY system is reported as 0.52 [17]. The RB $\phi_\Delta^1 O_2$ in PBS pH 7.4 is reported in the literature as 0.75 [21].

To advance the studies on the reaction between ABDA and singlet oxygen, the chemical rate constant (k_r) was determined using the first 180 s of the reaction. During this interval, the photobleaching of the dye is negligible, and the formation rates of $^1O_2$ can be considered constant. The equations applied in this step are described by Entradas et al. [22].

The singlet oxygen quantum yield was also determined directly from the near-infrared (1270 nm) phosphorescence emission of $^1O_2$ for the AA-containing systems. Data were obtained using a high-performance time-resolved fluorescence spectrometer, FluoTime 300 (PicoQuant, Germany). The phosphorescence decay lifetimes of singlet oxygen (τ^1O_2) were recorded using a time-correlated single-photon counting

setup. The decays were analyzed using the PicoQuant FluoFit Global Fluorescence Decay Analysis software. Phosphorescence decay curves at 1270 nm were recorded using a near-infrared photomultiplier tube, model H10330B (Hamamatsu, Japan). Irradiations were performed with a picosecond pulsed diode laser (LDH-P-635 driven by PDL 800-B, λ_{exc} = 635 nm, 80 MHz repetition rate, 72 ps pulse width, PicoQuant, Germany). Lifetimes were determined by applying a first-order fit to the phosphorescence decay curves. Equation (3) was used to determine $\Phi^1_\Delta O_2$.

$$\phi^1_\Delta O_{2\,PS} = \frac{Abs_S . I_{PS} . \tau_S}{Abs_{PS} . I_S . \tau_{PS}} \phi^1_\Delta O_{2\,S} \quad (3)$$

Where I is the area of the phosphorescence emission spectrum of singlet oxygen, Abs is the absorbance of the solutions at the excitation wavelength, and τ is the lifetime of singlet oxygen in the analyzed medium. The subscripts refer to the standard (S) and the photosensitizers (PS). Measurements were performed at 25 °C in D_2O as a solvent, and Azure A was used as standard ($\Phi^1_\Delta O_2 = 0.45$) [23].

2.6. Phototoxicity of formulations against Caco-2 cancer cells

Cell viability was assessed under both light and dark conditions using the MTT assay. For experiments conducted in the monolayer culture model, Caco-2 cells were seeded in 96-well plates at a density of 1.7 × 10^4 cells per well in complete medium supplemented with antibiotics. Cells were incubated for 24 h in a CO_2 incubator prior to treatment.

MTT assays were conducted after treating Caco-2 cells for 20 h with liposome samples, including: DPPC/F127/RBDEC/AA to evaluate the photosensitizers' combined actions, and individual DPPC/F127/AA and DPPC/F127/RBDEC to assess each photosensitizer's isolated effects. In all experiments, non-treated cells and cells treated only with empty DPPC/F127 hybrid liposomes were used as controls. The composition of each sample is detailed in the Supplementary information (Table S1).

After treatment, the wells were washed with MOPS buffer (200 μL/well), and the plates were exposed to warm white light (fluence: 24.0 J cm^{-2}) for 20 min, under normal atmospheric oxygen concentration. Immediately following the illumination period, the cells were incubated again for 2 h (37 °C and 5 % CO_2) with MTT salt (5 mg mL^{-1}, in DPBS buffer). The MTT solution was then discarded and DMSO (100 μL/well) was added. The plate was incubated again at 37 °C for 15 min to completely solubilize the formazan crystals. Absorbance was read at 540 nm using a microplate reader (FlexStation 3, Molecular Devices, USA). Dark controls were run concurrently with each experiment to ensure the observed effects were strictly photoactivation-dependent.

The number of viable cells was estimated and expressed as a relative percentage, with the mean of the control group set as 100 % cell viability. Each value is presented as the mean ± standard deviation (SD) of six independent measurements (n = 6). Due to the small sample size and the limitations this imposes on parametric statistical assumptions, all comparisons among groups were conducted using the non-parametric Kruskal–Wallis test, followed by Dunn–Bonferroni post hoc correction. The statistical significance was set at $p < 0.05$. Statistically significant differences are indicated by different letters in the graphs. All analyses were performed using RStudio software. Additionally, intracellular ROS generation assays were performed (data not shown) using the DCFDA (2′,7′-dichlorofluorescin diacetate) probe, indicating that all systems can produce reactive species.

The possible synergistic effect of the combined systems was evaluated using the non-linear statistics of dose-response curves of the Chou-Talalay method [24,25]. Caco-2 cell viability data observed in each isolated system, as well as in the combination at the different doses, were the values used in the calculations performed by the CompuSyn® software. The Combination Index (CI) isobologram was used to measure synergism, where CI values < 0.90 are synergistic, 0.90–1.10 are additive and CI > 1.10 are antagonistic effects [24,25].

2.7. Confocal microscopy and intracellular fluorescence lifetime

For subcellular localization experiments, glass coverslips (13 mm) were carefully positioned at the base of each well (24-well plate), and a precise quantity of 3 × 10^4 cells/well was seeded onto them. Subsequently, the cells were subjected to an incubation period of 48 h at 37 °C and 5 % CO_2 to cell adhesion. After this period, the cells were treated with a liposome formulation comprising both RBDEC and AA (1.0 × 10^{-6} mol L^{-1} for each compound) in DMEM medium supplemented with 10 % FBS, and the incubation was continued for 3 h. Following the incubation, the cells were washed twice with PBS at room temperature, followed by fixation with cold 4 % paraformaldehyde solution in PBS for 15 min. Additional washing steps with PBS were performed, and the coverslips were mounted onto glass slides using a prolonged mounting medium containing DAPI. Subsequently, the slides were allowed to incubate at room temperature for 15 min before undergoing confocal analysis. Excitation and emission (range) wavelengths used were, respectively, 405 nm and 415–450 nm for DAPI, 552 nm and 560–590 nm for RBDEC, and 638 nm and 675–750 nm for AA.

For fluorescence lifetime measurements, liposome formulations were prepared using either RBDEC or AA, due to their similar lifetimes. After treating the cells according to the confocal microscopy protocol, they were washed twice with PBS. Fluorescence lifetime measurements were performed using a PicoQuant MicroTime 200 time-resolved confocal fluorescence microscope (PicoQuant, Germany) equipped with a 20 × objective. RBDEC was excited using a 530 nm diode laser, and emission was collected through an HQ550LP filter. AA was excited using a 640 nm diode laser, and emission was collected through an HQ690/70m filter.

3. Results and discussion

3.1. Characterization of formulations after PS incorporation

The objective of this research was to develop a liposomal co-formulation containing the photosensitizers AA and RBDEC. These compounds have two distinguishing characteristics: they absorb at different wavelengths and exhibit large differences in lipophilicity. For comparison purposes, formulations containing the isolated PSs were also prepared. All systems achieved an average diameter between 30 and 50 nm, and an appropriate polydispersity index (PI < 0.30) after 360 s of sonication [26]. The prolonged sonication time is associated with the presence of bulky molecules, which prolong the bilayer organization time. A comparable outcome has been previously documented in liposomal systems containing fluorescein bound to F127 [27]. As observed in the TEM images (Fig. 2A), the DPPC/F127/RBDEC liposomes exhibited a well-distributed spherical morphology with an average diameter of 65.4 nm (Fig. 2B), consistent with the measurements obtained from DLS analysis (Table 1). The discrepancies observed between the techniques are attributed to the fact that DLS measures the hydrodynamic diameter. Moreover, the sample drying process on the grid - despite following a lyophilization protocol - can still cause vesicle deformation during drying. Without prior freezing and lyophilization of the grid, the TEM images presented staining artifacts due to RBDEC, as illustrated in the insert of Fig. 2A. Similar results were observed in the studies conducted by Bibi et al. [28] and Talmon et al. [29], which do not invalidate the characterization performed. In the case of the sample comprising both co-formulated dyes, the freezing and lyophilization process was conducted, effectively eliminating any staining effects (Fig. 2D). In conclusion, the data obtained from DLS and TEM analysis confirm that the interaction between F127 and DPPC is effective in maintaining the spherical shape and uniform size of the liposomes.

The diameters, polydispersity index (PI), and zeta potential of these formulations are presented in Table 2. Due to the presence of AA, the values of the zeta potential are positive because of the cationic nature of the phenothiazine dye. Although further studies are needed to infer the

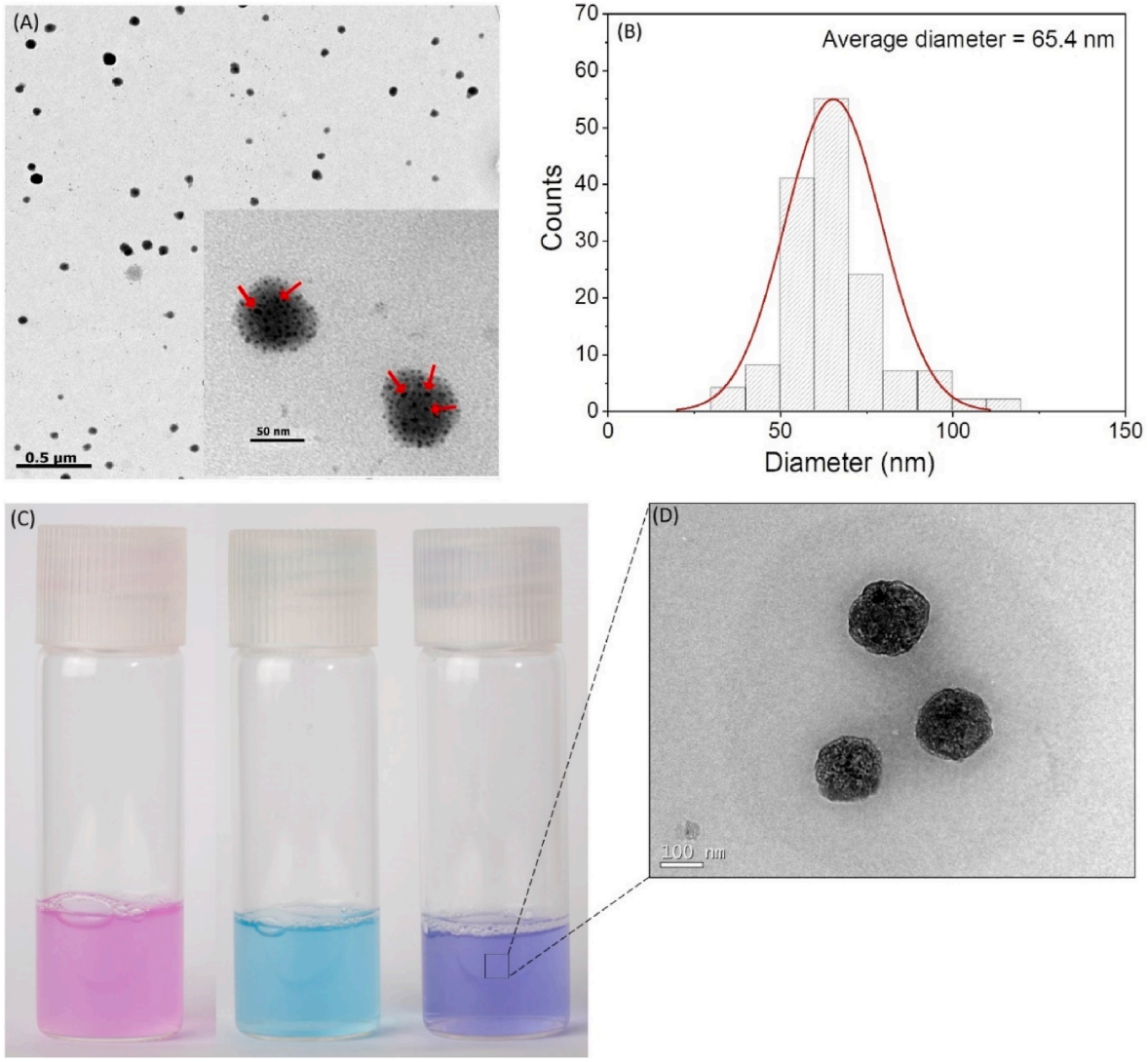

Fig. 2. (A) TEM images of the DPPC/F127/RBDEC sample; staining artifacts are highlighted in the insert; (B) Size distribution obtained from the microscopy images; (C) Photograph of DPPC/F127/RBDEC, DPPC/F127/AA and DPPC/F127/RBDEC/AA; and (D) TEM image of the combined system.

Table 1
Hydrodynamic diameter (D_H), polydispersity index (PI) and Zeta potential (ζ) of the samples. [AA] = 5.0×10^{-6} mol L^{-1} e [RBDEC] = 5.0×10^{-6} mol L^{-1}; pH 7.4 and 25 °C.

Sample	D_H (±SD)	PI	ζ (mV)
DPPC/F127	46.6 ± 2.4	0.267	−2.53
DPPC/F127/RBDEC	48.0 ± 0.2	0.277	−2.90
DPPC/F127/AA	30.8 ± 5.3	0.274	+8.51
DPPC/F127/RBDEC/AA	32.8 ± 5.9	0.284	+10.57

Table 2
Kinetic parameters of the encapsulation of RBDEC and AA by passive methodology into DPPC/F127 liposomes and of RBDEC added to the DPPC/F127/AA system; [AA] = 5.0×10^{-6} mol L^{-1} e [RBDEC] = 5.0×10^{-6} mol L^{-1}; pH 7.4 and 25 °C.

Sample/Kinetic parameters	k_1 (10^{-3} s^{-1})	k_2 (10^{-3} s^{-1})	R^2
DPPC/F127/RBDEC	9.43	0.74	0.997
DPPC/F127/AA	173.5	–	0.892
RBDEC into DPPC/F127/AA	124.7	2.24	0.947

position of AA, the zeta potential already indicates that it may be in a very outer position in the bilayer or even in the PEO layer. This result is expected since AA is an amphiphilic dye and at this concentration, it is still mainly monomerized [30].

Given the favorable solubility of Azure A at this concentration, its incorporation into the liposomal system is less probable than that of xanthenes. Accordingly, the encapsulation efficiency (EE%) was assessed by modifying the incorporation method. It is important to note that we used two methods of incorporation. What we call "passive addition" is done by adding PS into the liposome formulation. "Active addition" is done by incorporating PS at the thin film formation stage so that the dye is already in solution when the liposome is formed. Passive addition resulted in the incorporation of only 37.2 % ± 4.2 in the DPPC/F127/AA system, whereas active addition was able to encapsulate 54.6 % ± 4.1 of the phenothiazine. It is to be expected that hydrophilic dyes in liposomes have a lower EE% than highly hydrophobic compounds [31]. In the case of RBDEC, incorporation is essential due to its high hydrophobicity. The incorporation method was found to have little effect on its individual EE%, with average values of 97.6 % ± 0.2 being obtained. The simultaneous passive incorporation of both dyes in the combined system resulted in mutual interference, with EE values of 43.1 % ± 0.7 for AA and 70.6 % ± 0.2 for RBDEC. However, when AA was actively incorporated before the passive addition of RBDEC, optimal loading was achieved (AA = 60.3 % ± 0.1; RBDEC = 98.6 % ± 0.5).

Although the EE of AA under this active incorporation strategy differed slightly from that obtained when incorporated alone, statistical analysis (*t*-test, data not shown) indicated that these differences were not significant. This result could be related to the possible electrostatic interaction between the cationic AA and the phosphate group of DPPC, reducing the possibility of repulsion with the monoanionic RBDEC. Therefore, the active addition of AA and passive addition of RBDEC were used in all subsequent experiments. No purification steps were conducted to separate non-internalized content.

Concerning the spectral profile of the PSs in liposomes, it was observed that AA (Fig. 3C and D) exhibited characteristics analogous to those observed in aqueous media. It is noteworthy that the absorption spectrum is well-defined, with a minimal broadening signal [30]. It is possible that AA is in the aqueous well of the liposomes, or even in the PEO layer, which is a more hydrated region of the vesicle. Nevertheless, the most significant case is that of the highly hydrophobic RBDEC (Fig. 3A and B). Spectroscopic characterization demonstrated that RBDEC is incorporated into liposomes in its monomeric form. This is evidenced by the fluorescence emission profile, which is distinct and exhibits a markedly higher intensity than in other media. About this compound, the monomerization process is of particular significance to the cellular uptake, given that PS is predominantly self-aggregated in PBS. The observed increase in emission may be attributed to both the monomerization of the compound and its distance from water molecules. Moreover, the incorporation of RBDEC into liposomes resulted in a bathochromic shift in the absorption band, a phenomenon attributed to its allocation in an environment of reduced polarity [16].

The absorption spectrum of the combined system manifests as a combination of the RBDEC and AA spectra, as illustrated in Fig. S2. Several wavelengths (λ_{exc}) were evaluated to identify the optimal condition that did not imply, for example, the influence of internal filter effects. Fig. 4A depicts reference wavelengths in the absorption spectrum of the DPPC/F127/RBDEC/AA system, which facilitates comprehension of λ_{exc}.

The combination of the spectra of the compounds results in the inevitable excitation of the RBDEC, along with the AA, at $\lambda_{exc} < 610$ nm. While this characteristic may appear insignificant, it is of interest in combined systems to have distinct activation possibilities, i.e., wavelengths that activate the molecules separately and wavelengths that activate both compounds simultaneously. An increase in the excitation wavelength of AA results in a slight elevation in emission intensity, which subsequently attains a stable equilibrium at $\lambda_{exc} = 625$ nm. However, a notable bathochromic shift (approximately 24 nm) in the emission spectrum is also evident as λ_{exc} increases (Fig. 4B). It is established that the emission wavelength of a fluorophore is independent of the excitation region, a phenomenon known as Kasha's rule. Therefore, the spectroscopic profile identified for AA in the mixed system is somewhat exceptional and evades the conventional laws of fluorescence. According to Lakowicz [32], the phenomenon known as "red-edge excitation shift" (REES) can be observed in polar and viscous media when the solvent relaxation time becomes comparable to the fluorescence lifetime of the compound. In this case, excitation at longer wavelengths results in photoselection that excites fluorophores that are interacting more strongly with the solvent molecules [19,33]. The REES

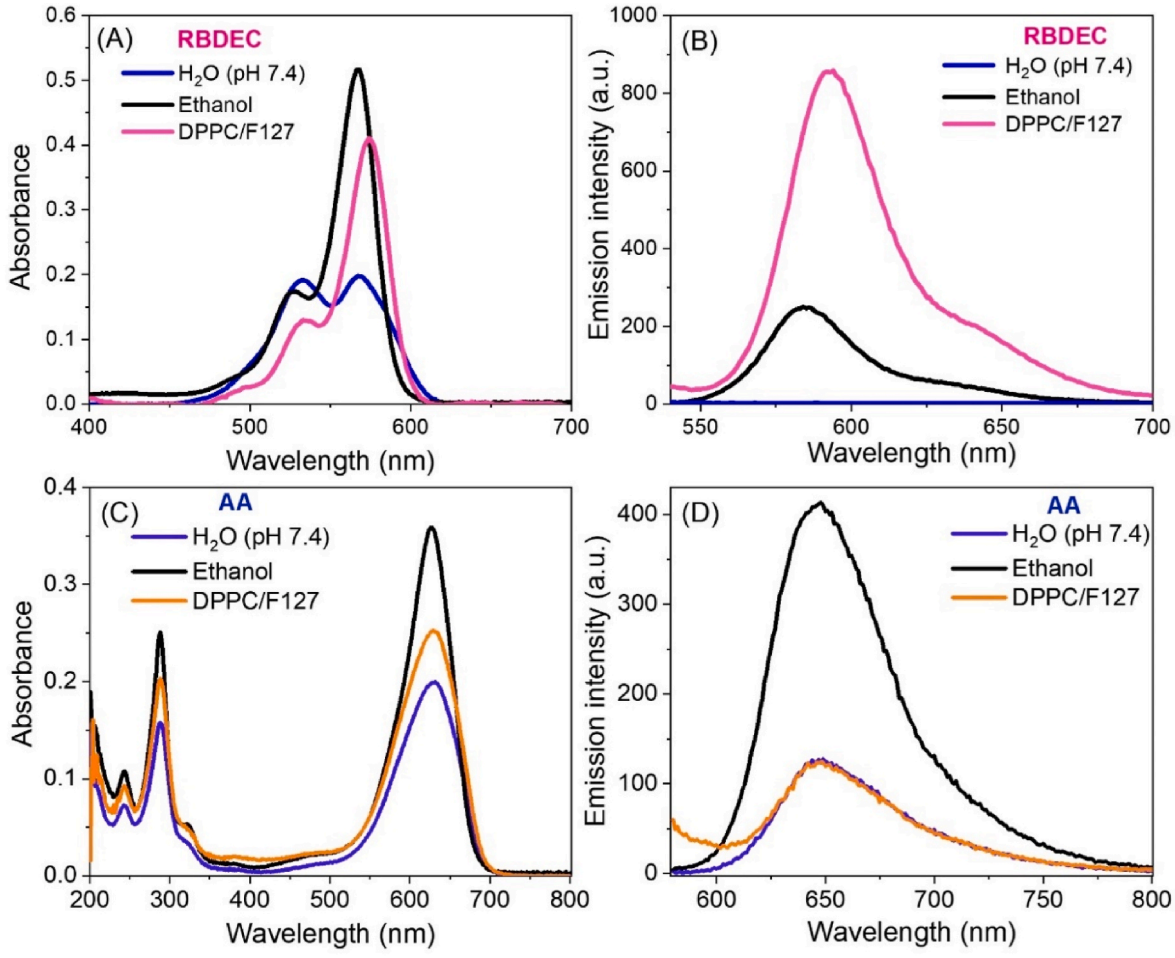

Fig. 3. Electronic absorption and fluorescence emission spectra of RBDEC (A and B) and AA (C and D) in PBS (pH 7.4 and [NaCl] = 0.15 mol L^{-1}), ethanol and DPPC/F127 liposomes; $\lambda_{exc} = 570$ nm; [RBDEC] = 5.0×10^{-6} mol L^{-1}, [AA] = 5.0×10^{-6} mol L^{-1} and 25 °C.

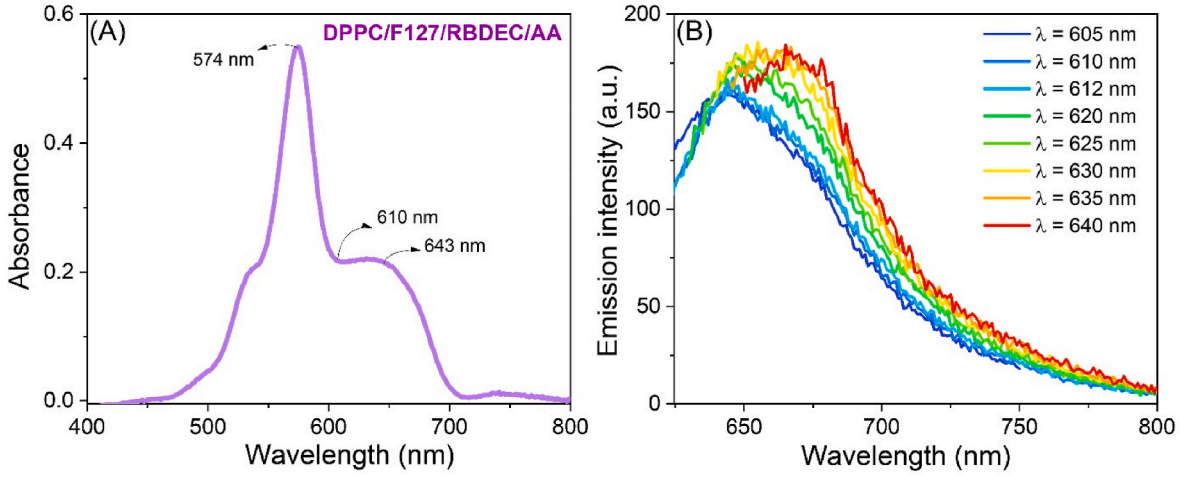

Fig. 4. Spectra of (A) electronic absorption of the DPPC/F127/RBDEC/AA sample and (B) fluorescence emission of the same system with different λ_{exc}; [AA] = 5.0 × 10^{-6} mol L^{-1} e [RBDEC] = 5.0 × 10^{-6} mol L^{-1}, pH 7.4 e 25 °C.

effect of the formulations will be examined later. It is important to highlight at this stage that the λ_{exc} for AA in combined systems was established as 610 nm, since this allows for a better definition of the spectrum, and the emission λ_{max} coincides with that observed in the DPPC/F127/AA sample. The spectroscopic analyses described above resulted in a series of findings regarding the systems, which are presented in the Supplementary information (Table S2).

The stability studies demonstrated that the formulations remained stable in solution for at least two months (Fig. S3). Moreover, following freeze-drying, all samples demonstrated stability for a minimum of one year. Upon rehydration after this period, they exhibited identical D_H, PI, and spectroscopic characteristics. As observed in previous studies on ERY [17] and RB derivatives [14], the samples allowed 10x and 100x dilutions in PBS while maintaining a D_H of 150 nm and a PI below 0.30. In oncological treatments, particle sizes under 200 nm are considered optimal due to the enhanced permeability and retention (EPR) effect [34]. These results highlight the significant potential of the system.

An increase in temperature did not result in a notable change in liposome diameter. These findings once again underscore the robustness of the DPPC/F127 hybrid liposomes [14]. However, the fluorescence emission of the compounds exhibited slight alterations, indicating a redistribution with increasing fluidity (Fig. S4). It is noteworthy that liposomes exhibit a phase transition temperature (T_m), wherein the membrane transitions from an ordered gel phase to a more fluid liquid-crystalline mesophase. The T_m of pure DPPC has been established at 41 °C [35]. In DPPC/F127 hybrid liposomes, however, the T_m is considerably broader, beginning at around 37 °C. The fluorescence emission of RBDEC was observed to exhibit a continuous increase up to 40 °C, followed by a slight reduction at higher temperatures. It is postulated that the observed increase in fluorophore emission is associated with the continuous enhancement in bilayer fluidity, which potentially facilitates more efficient distribution of the PS molecules. At a certain point, the fluidity is so great that water molecules begin to access the bilayer. Consequently, fluorescence quenching processes once again reduce the PS emission, as observed by Neunert et al. [36] However, in the system described here, the emission reduction is minimal, suggesting that the entry of water may be impeded by the presence of F127 molecules. Additionally, it was noted that the fluorescence emission did not fully recover to its original value following a cooling process to 25 °C. It is conceivable that the enhancement in the fluidity of the bilayer and the subsequent transition to the gel phase prompted the relocation of the PS. However, this phenomenon does not impede the applicability of RBDEC, as even with minor fluctuations, the fluorescence emission spectrum remains well-defined, indicating that the PS remains monomerized.

Furthermore, it is observed that despite the phase transition of the liposomes, the variation in fluorescence emission of AA in the system where it is isolated is minimal. This outcome suggests that the distance of PS from the lipid chains renders it less susceptible to inherent changes. Finally, in the combined system we evaluated both PSs according to their λ_{exc}. In this instance, RBDEC exhibited the same behavior previously described. Interestingly, AA in this formulation exhibited the same behavior as RBDEC, which differed from that observed in its isolated system. In this case, it appears that the AA is detecting a change in the distribution of the xanthene. It is plausible that an energy transfer occurs between the PSs in the combined system.

3.2. *Evaluating the interaction between PS and liposome*

Evaluating the interaction of PS in a combined system is challenging due to potential concurrent interactions. To address this, each PS was first assessed individually for its interaction with liposomes, followed by evaluation within the combined system. The encapsulation kinetics of each PS into the DPPC/F127 liposomes were evaluated. Subsequently, the encapsulation kinetics of RBDEC into the DPPC/F127/AA formulation were studied. This experiment precisely mimics the proposed method of preparing the combined formulation, with active addition of AA and passive addition of RBDEC. The kinetic parameters obtained are presented in Table 2 and the graphs are presented in Supplementary Material (Fig. S5).

The encapsulation kinetics of AA and RBDEC into liposomes differ significantly. AA follows a first-order monoexponential kinetic profile, whereas RBDEC exhibits a slower, two-step internalization process. The faster, monoexponential encapsulation of AA aligns with previously reported findings for Rose Bengal (RB), another amphiphilic PS [14]. These results suggest that the encapsulation kinetics of PS into liposomes are strongly influenced by molecular volume and hydrophobicity. Bulky and highly hydrophobic compounds like RBDEC exhibit a slower internalization process, as they diffuse more slowly through the medium and require monomerization.

The most intriguing result was observed in the encapsulation of RBDEC within a system that already contained AA. In this case, the kinetic model still fits a first-order bi-exponential equation, but the rate constants are significantly higher. This faster encapsulation of RBDEC is hypothesized to result from electrostatic attraction due to the positive surface potential of the DPPC/F127/AA system (ζ = +8.51 mV).

The release kinetics of the PSs were also evaluated at physiological and mildly acidic conditions (simulating the tumor microenvironment)

[37]. The results showed that RBDEC release did not exceed 3.5 % during the 3-h analysis period across all systems examined. In contrast, the release of AA was evident within the first minutes of the experiment. This behavior is likely due to the external localization of the PS, presumably within the PEO layer, and its amphiphilic nature, which accentuates the release of the phenothiazine. The release profile of AA at physiological pH is shown in Fig. S6B, indicating that its release is approximately twice as high in the DPPC/F127/RBDEC/AA system compared to the system containing isolated AA. A similar trend is observed under mildly acidic conditions, although the difference between the two systems is less pronounced. Kinetic modeling revealed that the release follows first-order kinetics, being concentration-dependent rather than diffusion-controlled, as described by the Higuchi model. Despite this, the first-order rate constants are comparable in both cases. Considering the zeta potential values, the incorporation of RBDEC may slightly alter the localization of AA, possibly positioning it closer to the outer regions of the carrier and thus facilitating its release under these conditions.

3.3. Estimation of PS position in the liposomal structure

In order to confirm the external location of AA and its different position in isolated or combined systems, the Stern-Volmer plots are performed with iodide acting as a water-soluble quenching agent. Table 3 presents the results of Stern-Volmer constants (K_{SV}). The results indicate that the quenching of AA is initially more pronounced in the combined system compared to the DPPC/F127/AA sample. This observation suggests that the phenothiazine molecule may adopt a more external position in the presence of RBDEC. Interestingly, a segment of the Stern-Volmer plot for AA in the combined system exhibits a reduced slope, leading to the calculation of a second K_{SV} value. As reported in the literature [27], such a profile may correspond to a secondary population of PS molecules located in a distinct region within the liposome structure.

As expected, the quenching of AA is significantly greater than that of RBDEC. This finding implies that the xanthene is positioned in a more internal region, aligning with its hydrophobic characteristics. Moreover, the incorporation of RBDEC into the combined system, whether passive or through active addition in DPPC/F127/RBDEC, appears to be comparable.

To gain deeper insights into these issues, a Förster resonance energy transfer (FRET) experiment using DPH as an energy transfer probe [19,38] was also conducted. FRET is a technique that enables the estimation of the distance between two fluorophores in a medium. This phenomenon can be observed when energy transfer occurs between a donor and an acceptor molecule at a distance of up to 10 nm. According to the theory [19], a critical aspect is the overlap of the emission spectrum of the energy donor with the absorption spectrum of the acceptor. In the presented case, both PSs exhibit an overlap with the emission spectrum of DPH, as illustrated in Fig. S7. DPH is known to present good spectral overlap with xanthenes [38] and to have its location well determined in DPPC liposomes [39,40]. Repáková et al. [40] have demonstrated that DPH is located in the center of the bilayer, perpendicular to the carbon chains.

Table 3
Stern-Volmer constant (K_{SV}) of fluorescence quenching of formulations by the addition of iodide ion. [AA] = 5.0×10^{-6} mol L^{-1}; [RBDEC] = 5.0×10^{-6} mol L^{-1}; pH 7.4 and 25 °C.

Sample	K_{SV} (1)	K_{SV} (2)	R^2
DPPC/F127/RBDEC (active)	0.48 ± 0.03	–	0.941
DPPC/F127/RBDEC (passive)	0.86 ± 0.03	–	0.955
DPPC/F127/AA	6.74 ± 0.10	–	0.995
DPPC/F127/RBDEC/AA (λ_{exc} = 610 nm)	9.04 ± 0.18	2.58 ± 0.83	0.994
DPPC/F127/RBDEC/AA (λ_{exc} = 520 nm)	0.43 ± 0.04	–	0.884

The results demonstrated that the incorporation of RBDEC resulted in a reduction of the fluorescence emission of DPH and the emergence of the dye emission band at 595 nm, indicative of energy transfer (Fig. 5A). In this instance, the distance between DPH and RBDEC was determined to be 37.2 Å. A comparison of this result with the results found for the DPPC/F127/RB and DPPC/F127/RBBUT systems described in the literature (r = 33.3 Å and 30.7 Å, respectively) reveals that the distribution observed does not align with the expected logic of hydrophobicity [14]. The calculated distance indicates that RBDEC is situated at a greater distance from DPH and, consequently, in closer proximity to the aqueous interface than the other xanthenes. To explain this unexpected result, it is proposed that this minor discrepancy is associated with the length of the ester chain (10 carbons, ~11.34 Å) and that it ultimately causes DPH to move away from the chromophoric region of RBDEC. Moreover, the substantial length of the alkyl chain may contribute to the molecule's role as a "co-surfactant," facilitating the stabilization of the bilayer. Consequently, even after reaching equilibrium, the molecule is positioned with its xanthene group oriented towards the interface [16].

To ascertain the location of AA within the systems, two experiments were devised. In the initial experiment, the position of AA was evaluated in a formulation comprising solely DPPC/F127 and the DPH probe (Fig. 5B). In the subsequent experiment, in addition to DPH, the presence of RBDEC (5.0×10^{-6} mol L^{-1}) was also maintained (Fig. 5C). In Fig. 5B, it is evident that the energy transfer is considerably reduced, despite the slight decline in DPH emission, which is almost indiscernible. Conversely, the rise in AA emissions is virtually imperceptible. This suggests that the position of AA is significantly separated from that of DPH. As previously discussed, the available evidence suggests that AA is located in the PEO layer resulting from the addition of F127 to the liposomes. Fig. 5C also depicts a slight decline in DPH emission, although, in this instance, the baseline emission was already relatively low. This phenomenon occurs because in this experiment RBDEC was already present in the formulation, and it is established that there is an energy transfer between the DPH-RBDEC pair. The distances determined through the application of the FRET equations were 53.9 Å for AA in the DPPC/F127 system and 54.3 Å in the combined system. The discrepancy is minimal, yet it may suggest the most external position of AA when RBDEC has already assumed a position within the bilayer. Although the values are very close, it can be stated that the FRET results follow those obtained from fluorescence quenching.

Fig. 5C reveals a further noteworthy observation: the RBDEC emission decreases as AA is introduced into the system. Indeed, the spectroscopic characterization revealed that the fluorescence yield of RBDEC in the combined formulation was observed to be lower than in its isolated system. One potential explanation for this outcome is the transfer of energy from RBDEC to AA, given the significant overlap between the xanthene emission and the phenothiazine absorption. To assess this phenomenon, the DPPC/F127/RBDEC system was employed as an energy donor, with successive additions of AA. The results are illustrated in Fig. 5D. The addition of AA resulted in a continuous decrease in the RBDEC emission, as well as the appearance of a band at 650 nm, which corresponds to the AA emission. The results demonstrate that energy transfer occurs between the two PSs, which ultimately reduces the fluorescence quantum yield of RBDEC. Once more employing the FRET equations, it is calculated that the distance between the RBDEC-AA pair is 18.0 Å. Given that the values for the DPH-RBDEC distance were 37.2 Å and DPH-AA were 54.3 Å, it is deemed that this value is consistent with the preceding results and serves to reinforce the position of the AA in the PEO layer.

Among the findings about the spectral profiles of the formulations, the most intriguing was observed in Fig. 4B. Following Kasha's rule, the fluorescence emission of a fluorophore is independent of λ_{exc} [19]. However, as evidenced by the data, the variation of the λ_{exc} of the AA in the combined system resulted in emission spectra with different λ_{max}. To elucidate the impact of varying excitation wavelengths, spectra were also obtained for the RBDEC in the DPPC/F127/RBDEC/AA and

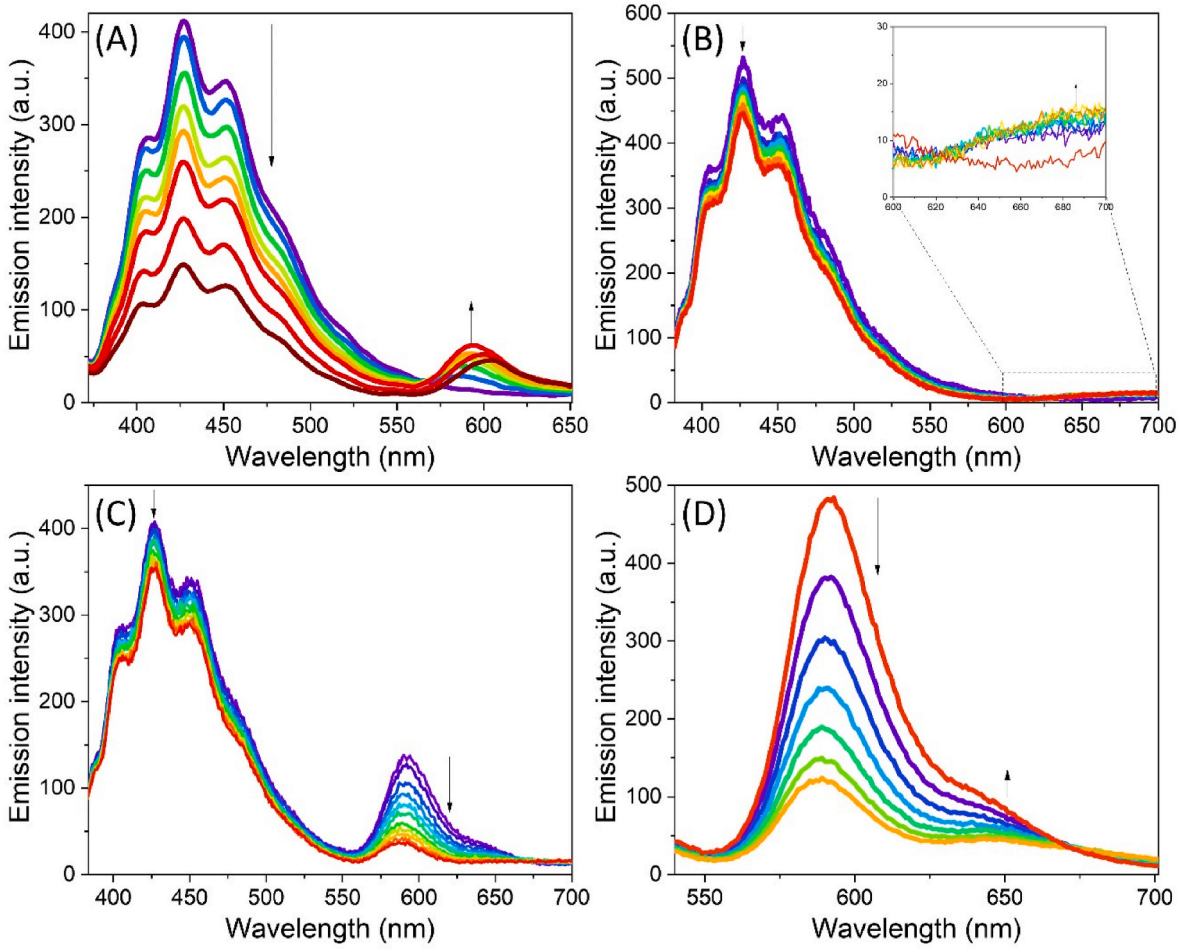

Fig. 5. FRET between DPH and (A) RBDEC and (B) AA with DPPC/F127; (C) FRET between DPH and AA in DPPC/F127/RBDEC and (D) Fluorescence emission of RBDEC with the addition of AA (arrows indicate intensity variation as PS is added). [PS] = 5.0×10^{-6} mol L^{-1}; pH 7.4 and 25.0 °C. $\lambda_{exc,DPH}$ = 380 nm where the dye does not absorb.

DPPC/F127/AA formulations. The wavelengths at the maximum emission were plotted in relation to the excitation wavelength and are illustrated in Fig. 6.

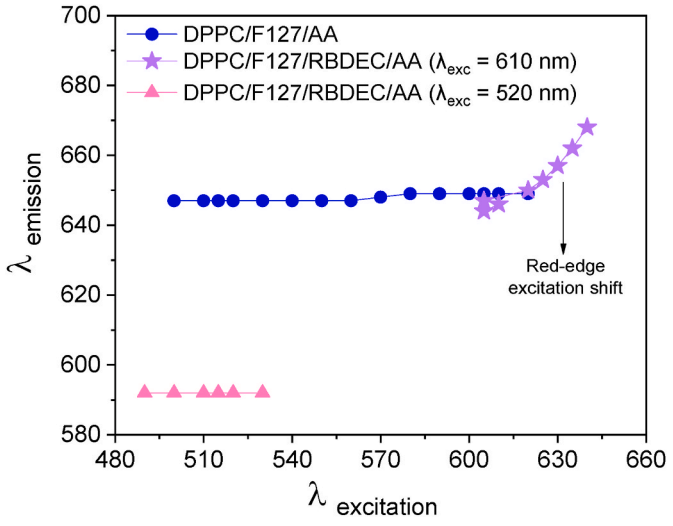

Fig. 6. Maximum emission wavelength as a function of excitation wavelength for AA and RBDEC dyes in liposomal formulations. [AA] = 5.0×10^{-6} mol L^{-1} and [RBDEC] = 5.0×10^{-6} mol L^{-1}; pH 7.4 and 25 °C.

As postulated by Lakowicz [32], the presence of polar fluorophores in polar and moderately viscous solvents results in incomplete solvent relaxation, which in turn gives rise to a shift in the fluorescence emission spectrum. This shift represents a photoselection phenomenon, whereby molecules that are strongly bound to the solvent are preferentially excited. The phenomenon has been employed in studies of protein dynamics and the location of fluorophores in membranes [19,32,33,41]. The phenomenon known as REES has already been employed, for instance, to examine the mobility of lipid bilayers [42] and the position of a fluorescent probe in DPPC liposomes [43]. As investigated in these studies, parameters such as polarity, mobility, intermolecular interactions, and extent of water penetration vary as a function of the depth of the bilayer. The same explanation extends to hybrid liposomes that also have a hydration layer due to PEO groups on the surface. The restriction of polar solvents' mobility in high-viscosity media ultimately results in a reduction of their relaxation time to a duration comparable to that of the fluorescence lifetime of the fluorophore [33]. Consequently, the time required for reorganization into the excited state is absent, and fluorescence emission is contingent upon the excitation wavelength.

To gain a better understanding of how the REES effect was identified exclusively for AA in DPPC/F127/RBDEC/AA, the fluorescence lifetimes of each system were obtained. In the combined system, RBDEC excitation produced a fluorescence lifetime of $\tau_F = 1.551$ ns ($\chi^2 = 1.124$). For AA in DPPC/F127/AA (λ_{exc} = 635 nm), the values were $\tau_F = 1.277$ ns (23.75 %) and 0.657 ns (76.25 %), with $\chi^2 = 1.082$, and for AA in combined system $\tau_F = 0.754$ ns (22.99 %) and 0.344 ns (77.01 %), with

$\chi^2 = 1.078$. The findings indicated that both samples containing the phenothiazine dye exhibited two distinct populations. It is conceivable that the faster population may be AA in the bulk solution ($\tau_F = 0.4$ in water [44]), while the remainder may be AA incorporated into the liposome. It is also observed that the τ_F of AA decreases by approximately 50 % when it is in the presence of RBDEC. The fluorescence lifetime decrease observed for AA within the liposomal structure suggests its position is more susceptible to quenching by water molecules. However, the viscosity imposed by the PEO chains attached to the lipid bilayer likely restricts water molecule mobility in this region. Consequently, the solvent's relaxation lifetime is nearly equivalent to AA's fluorescence lifetime, leading to the REES effect. In the DPPC/F127/AA formulation, AA is more internalized and exhibits a longer fluorescence lifetime, providing sufficient time for the reorganization of solvent clusters. Fig. 7 illustrates the proposed location of AA in the formulations, based on the analysis of the REES effect.

3.4. Photophysical properties

A key aspect of PDT is the generation of singlet oxygen ($^1O_2$) within the liposome, which can then diffuse to the exterior to reach the target cell. To estimate this photophysical behavior, an indirect methodology utilizing the ABDA probe was employed. Table 4 presents the values of k_r, k_{PB}, and k_{ABDA}, along with the number of photons absorbed over 360 min (N_{ABS}), chemical photodynamic efficiency (γ_Δ), and the quantum yield of singlet oxygen ($\phi^1_\Delta O_2$).

As previously described [14], in the assays involving ABDA, a period of 1 h was allowed to elapse before the commencement of the illumination. This period is necessary to ensure equilibrium in the diffusion of ABDA into the liposomal vesicles. Moreover, to calculate $\phi^1_\Delta O_2$, the standard was maintained in a medium that was consistent with that of the sample. In other words, for liposomal systems, the standard used was the DPPC/F127/ERY system, the $\phi^1_\Delta O_2$ of which was determined by direct methodology [17].

In an aqueous medium, RBDEC exhibits a negligible yield of $^1O_2$, a phenomenon attributed to its propensity for self-aggregation in this environment. Self-aggregation suppresses excited states and consequently affects the generation of singlet oxygen. On the other hand, the DPPC/F127/RBDEC sample showed $\phi^1_\Delta O_2$ 160 times higher. This demonstrates the great advantage of using this encapsulated PS in a delivery system. The monomerization of RBDEC, achieved after its distribution in the lipid bilayer, provided a longer lifetime of the triplet state and consequently a greater generation of singlet oxygen.

Both the k_{ABDA} and k_r values are significantly elevated for AA, which can be attributed to its cationic nature. This positive charge facilitates closer interactions with the tetraanionic ABDA molecule, reducing alternative deactivation pathways for singlet oxygen ($^1O_2$) and increasing the probability of reaction with the probe. Additionally, the emission spectrum of the light source overlaps more effectively with the absorption of AA-containing samples (appsec1), leading to a higher photon absorption rate for these formulations.

In liposomal systems, the combined system exhibited a lower singlet oxygen quantum yield compared to the other formulations. This reduction can be attributed to the experimental method's limitations, as the positive charge of AA likely draws ABDA closer, potentially diverting $^1O_2$ generated by RBDEC into alternative deactivation routes. Furthermore, energy transfer between the PSs in the combined system slightly diminishes photodynamic activity.

Interestingly, the combined system demonstrated a notable reduction in photobleaching for both PSs. Despite the lower immediate yield, this effect may enhance the system's overall photodynamic application by extending the duration of its activity, presenting a potential

Table 4
Photophysical and reaction parameters were obtained for DPPC/F127/RBDEC, DPPC/F127/AA, and DPPC/F127/RBDEC/AA after reaction with the ABDA probe. [PS] = 5.0×10^{-6} mol L^{-1}, [ABDA] = 6.0×10^{-5} mol L^{-1}; pH 7.4 and 25 °C.

Sample	k_r (10^4 m^{-1} s^{-1})	k_{PB} (10^{-4} s^{-1})	k_{ABDA} (10^{-3} s^{-1})	N_{ABS} (10^{-4} E)	γ_Δ	$\phi^1_\Delta o_2$
RBDEC (PBS, pH 7.4)	3.47	0.67	0.15	3.89	0.38	0.003
DPPC/F127/RBDEC	0.60	2.58	4.35	1.32	32.95	0.48
AA (PBS, pH 7.4)	6.13	1.21	18.4	2.47	74.5	0.45[a]
DPPC/F127/AA	3.85	0.90	13.0	3.78	34.4	0.50
DPPC/F127/RBDEC/AA	3.58	0.14 (AA); 0.86 (RBDEC)	9.89	4.48	22.1	0.32
DPPC/F127/ERY	0.42	3.66	3.33	0.93	35.70	0.52[b]

k_r: chemical reaction rate constant (180 s); k_{PB}: photobleaching rate constant; k_{ABDA}: ABDA photodegradation rate constant; N_{ABS}: number of photons absorbed; γ_Δ: chemical photodynamic efficiency; $\phi^1_\Delta o_2$: singlet oxygen quantum yield.
[a] Value obtained in reference. [23].
[b] Used as a standard for liposomal systems, value determined in reference. [17].

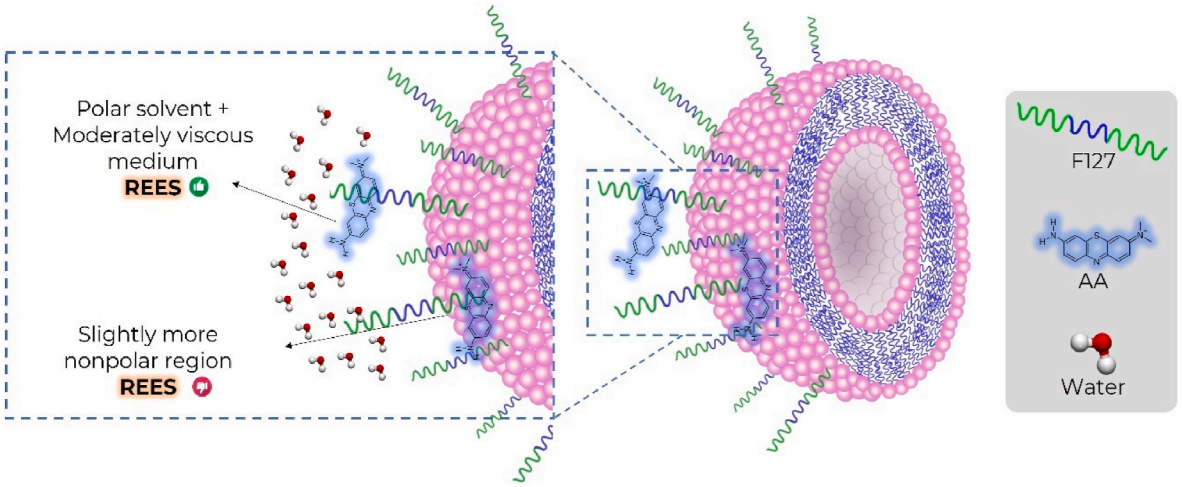

Fig. 7. Representation of the proposed location for AA in the different formulations.

advantage over other formulations.

To address the limitations of the indirect method, we also assessed the $\phi_{\Delta}^{1}O_2$ using a direct approach by following the $^1O_2$ near-infrared phosphorescence at 1270 nm. The lifetime of $^1O_2$ was determined to be 5.26 μs in D_2O, 8.87 μs in DPPC/F127/AA, and 8.22 μs in DPPC/F127/RBDEC/AA using first-order kinetics fitting. These values for the liposomal systems were found to be consistent with those previously presented by Freitas et al. [17]. The observed increase in the lifetime of singlet oxygen following the incorporation of PS into liposomes can be attributed to its protective effect against collisional processes that would otherwise lead to non-radiative decays.

The results demonstrated a quantum yield of 1.20 for DPPC/F127/AA and 0.74 for the combined system. While the values differed according to the methodology employed, it was observed that in both cases, DPPC/F127/AA exhibited a higher generation of singlet oxygen. Moreover, the direct methodology revealed a markedly elevated $^1O_2$ generation in the DPPC/F127/AA system, even when compared to AA in an aqueous medium. This finding substantiates the remarkable photodynamic potential of the formulation. Regarding the combined system, the decrease in yield of about 38 % is probably related to the energy transfer between RBDEC and AA. This result does not make the application of this formulation impossible, since it is known that liposomes are internalized in the intracellular environment and thus can deliver PS to different organelles.

3.5. Photodynamic activity and dynamics of PS interaction with cancer cell

The undifferentiated human colorectal adenocarcinoma cell line Caco-2 is among the most extensively utilized in vitro models for evaluating the cytotoxic effects of compounds with potential application as anticancer drugs [45]. In the present study, this cell line was used to investigate the photodynamic effects of the proposed formulations. To evaluate the cytotoxic potential of each system, treatments were carried out under both light-activated and dark conditions. Cell viability was quantitatively measured using the MTT colorimetric assay, a widely accepted method for assessing metabolic activity as an indicator of cell viability and cytotoxicity. The results of these experiments are shown in Fig. 8.

It is important to note that the DPPC/F127 formulation, when used alone, did not demonstrate any cytotoxic effects on Caco-2 cells. Moreover, formulations containing AA significantly reduced cell viability, even in the absence of light. As shown in Fig. 8A, all samples with AA in their composition exhibited a significant difference compared to the control ($p < 0.05$). The cytotoxicity of phenothiazines has been previously documented in studies involving methylene blue [46,47] and is attributed to disruption of mitochondrial energy metabolism, which induces oxidative stress and leads to cell death [48]. Klosowski et al. [49] recently demonstrated that the novel methylene blue derivative (NMB) exhibits dark cytotoxicity, attributed to its strong affinity for cellular membranes and its capacity to interfere with cellular redox and energy pathways. In particular, NMB targets mitochondria, where it disrupts oxidative phosphorylation, leading to the collapse of the electrochemical gradient, oxidation of NADH, and the subsequent release of mitochondrial enzymes. Notwithstanding this outcome, the photodynamic effect is evident, as illustrated in Fig. 8B. A statistical analysis of multiple comparisons revealed a substantial decline in cell viability following illumination for all samples containing PS above 5×10^{-6} mol L^{-1} in comparison to the control group ($p < 0.05$). In the case of the combined samples, a reduction in cell viability of 79.4 % ($p < 0.05$) and 87.4 % ($p < 0.0001$) was observed at concentrations of 2.5×10^{-6} mol L^{-1} and 5.0×10^{-6} mol L^{-1}, respectively.

While the objective of this research was the development of a combined system, the results presented in Fig. 8 do not indicate a synergistic effect. This is evidenced by the inactivation percentages of the DPPC/F127/RBDEC (5.0×10^{-6} mol L^{-1}) system (82.3 % ± 3.0), DPPC/F127/AA (5.0×10^{-6} mol L^{-1}) (80.8 % ± 6.9), and the combined system (2.5×10^{-6} mol L^{-1}) (79.4 % ± 5.8). The observed difference between these groups is not statistically significant, as can be seen in the data. The use of combined systems has gained attention as a promising approach in cancer treatment, offering potential advantages such as dose reduction, lower toxicity, and decreased cellular resistance [50]. While the concept of "synergism" is interpreted variably in the literature, Chou [24] emphasizes that it encompasses more than a simple additive effect. Chou

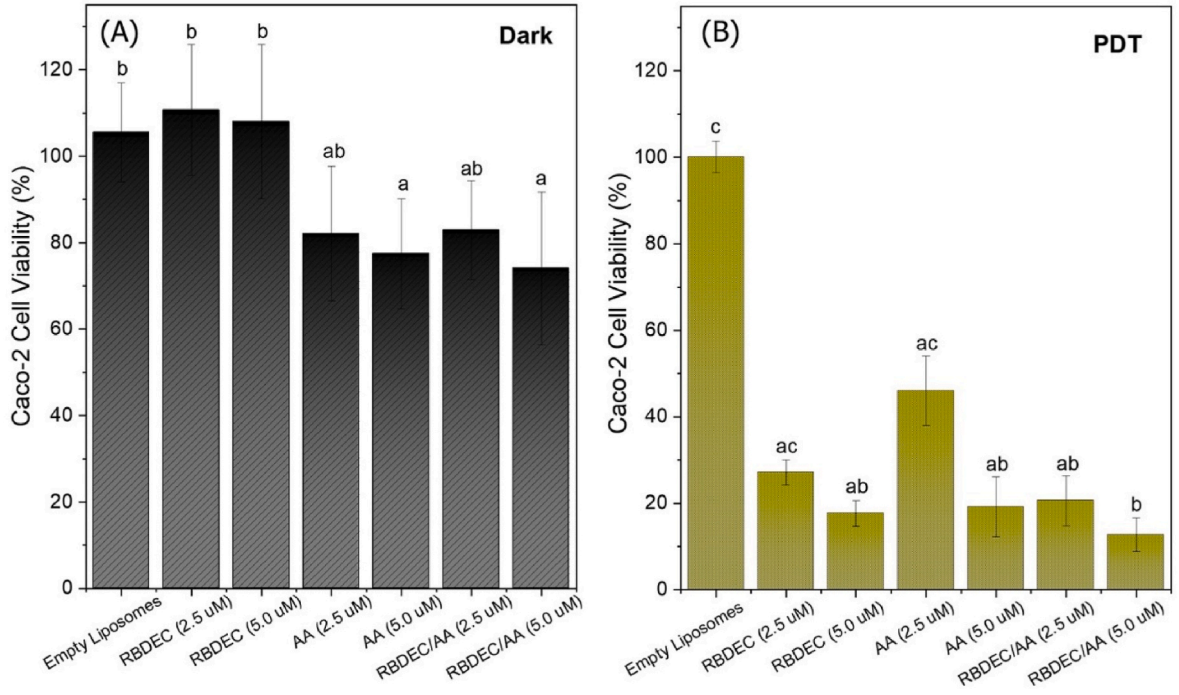

Fig. 8. Photodynamic activity of the different liposomal formulations against Caco-2 cancer cells; (n = 6) ± SD. Different letters indicate statistically significant differences ($p < 0.05$).

and Talalay [51] developed the "Combination Index" (CI) to quantify interactions between agents. According to this model, CI values below 0.9 indicate synergism, values above 1.10 indicate antagonism, and values between 0.90 and 1.10 reflect an additive effect. Applying this framework to the current study produced the graph shown in Fig. S8. The formulation containing 5.0×10^{-6} mol L^{-1} of each compound displayed a moderate antagonistic effect, whereas the sample with the lowest concentration exhibited an additive effect. These results indicate that the interaction between the compounds is concentration-dependent, showing a tendency toward synergistic effects at lower concentrations.

It can be postulated that since the liposome was internalized without the release of the dyes, the energy transfer between the PSs was maintained, which has the effect of hindering the photodynamic activity of the system. Nevertheless, if liposome internalization occurs with the intracellular release of PSs, the distinction in classes, lipophilicity, and electrical charges of the compounds may result in their migration to different intracellular compartments. As documented in the literature [52], positively charged molecules tend to accumulate in mitochondria, while negatively charged molecules are transported to lysosomes due to the opposing electrochemical potentials of these organelles. To further investigate these possibilities, the distribution of RBDEC and AA in Caco-2 cells was investigated through the use of confocal microscopy images. Future studies should include co-localization experiments with organelle-specific fluorescent markers, combined with quantitative image analysis, to better define the intracellular localization of RBDEC. The results of this experiment (Fig. 9) demonstrated a significant overlap between RBDEC and the DAPI image, indicating that RBDEC is predominantly localized within the nucleus region of the cells. It is a well-established fact that the nucleus contains the majority of the intracellular genetic material. The targeting of drugs in this region enables them to exert their therapeutic effect by acting directly on the DNA strands [53]. In contrast, confocal imaging of AA demonstrated a dispersed distribution within the cytoplasm, with a notable accumulation observed in the perinuclear region. This distribution may be attributed to the cytoplasm water content, which creates a more propitious environment for AA [54]. This contrasting distribution of the drugs suggests the possibility of targeting distinct cellular sites for therapeutic interventions utilizing a photocytotoxicity approach, thereby enhancing the overall efficacy of therapy. An additional benefit of the developed systems is their ability to optimize the use of the light source. The incorporation of distinct PSs has been demonstrated to augment the absorption of photons from the white LED, thereby potentiating the photodynamic effect. As previously mentioned, positively charged molecules have been observed to accumulate in mitochondria with a higher degree of preference. In the context of PDT, this interaction is of significant importance, since photodamage to mitochondria initiates an apoptotic cascade [55]. It is also worth noting that studies have shown that mechanisms initiated in specific organelles, such as lysosomes, can enhance the efficacy of PDT [56]. Therefore, further studies aimed at defining the specific location of PSs, including lysosomes and mitochondria, should be considered for a more accurate assessment.

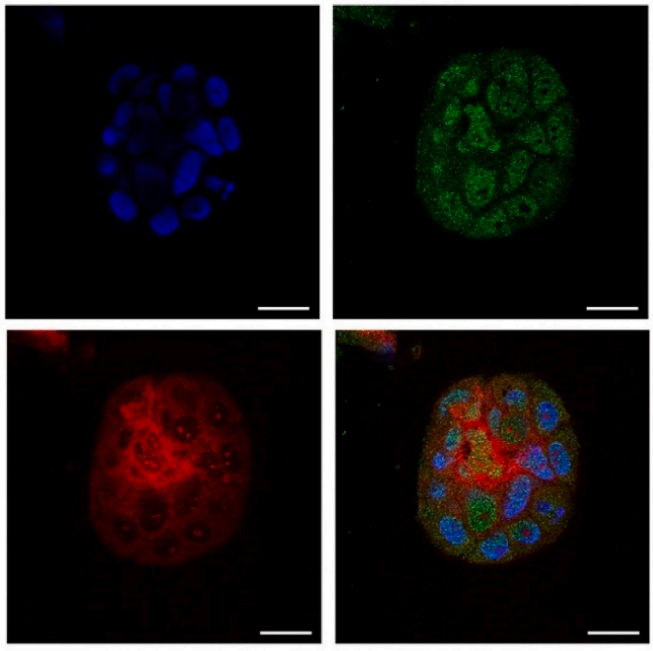

Fig. 9. Confocal microscopy images of U251 incubated for 4 h with DPPC/F127/RBDEC/AA. Blue: DAPI; Green: RBDEC; RED: AA. [RBDEC] and [AA] equal to 1.0×10^{-6} mol L^{-1}. Scale bar = 25 μm. (For interpretation of the references to color in this figure legend, the reader is referred to the Web version of this article.)

Furthermore, fluorescence lifetime measurements were obtained for each of the PSs in the intracellular medium. Three fluorescence lifetime components were observed for RBDEC (Table 5). The chi-square (χ^2) values around 1 and the random distribution of residuals reinforce the data. The longest lifetime appears to be associated with monomeric species. Previous studies have demonstrated a monomer lifetime of approximately 6–7 ns for RB [57]. The lifetime of around 2 ns appears to be related to small self-aggregated species such as dimers, while the shortest lifetime (<1 ns) could be due to the presence of larger self-aggregated species such as trimers and tetramers. This has been observed for other photosensitizers within the intracellular milieu as well [54,58]. The fractional intensity (f_a) indicates that less than 10 % is attributed to monomeric species (f_1), while the majority is related to self-aggregated species (f_2+f_3). This may be due to the highly hydrophobic nature of the dye, which seems to favor its self-aggregation in the intracellular environment. Furthermore, the presence of RBDEC in the nuclear region could lead to a bound to the grooves of DNA bases, promoting self-aggregation [59]. For AA, two lifetimes were observed, which were respectively related to monomers and self-aggregated states of the PS [30], similar to what was discussed for RBDEC.

4. Conclusions

The present study details the design of a dual-target liposomal system intended for a multicellular approach to photodynamic therapy against colorectal cancer cells. Initially, the hydrophobic RBDEC and the hydrophilic AA photosensitizers were successfully co-encapsulated in small unilamellar vesicles of DPPC/F127. The DPPC/F127/RBDEC/AA vesicles have a hydrodynamic diameter (D_H) of approximately 30 nm, a polydispersity index (PI) of 0.28, and exhibit excellent temporal, thermal, and dilution (x100) stability. Active incorporation of AA followed by passive encapsulation of RBDEC results in approximately 60 % entrapment of AA and 98 % entrapment of RBDEC. Stern-Volmer and FRET assays reveal that RBDEC is located closer to the aqueous interface due to interaction between its decyl chain and the lipid bilayer. These assays, along with the red-edge excitation shift (REES effect), confirm that AA is mostly located externally, near the PEO groups of F127. The combined system was tested against Caco-2 cancer cells, showing promising results by reducing cell viability by approximately 80 % after 20 min of illumination (white LED, 24.0 J cm^{-2}). The Chou–Talalay combination index indicated an antagonistic effect (index = 1.39) for the dyes at higher concentration ($5.0x10^{-6}$ mol L^{-1}). However, at a lower concentration ($2.5x10^{-6}$ mol L^{-1}), an additive effect was observed (index = 1.09), suggesting that future studies exploring combined systems at lower concentrations may promote a synergistic effect. Confocal microscopy images of Caco-2 cells showed distinct localizations of both AA and RBDEC, with AA localized in the cytoplasm and RBDEC at the nucleus region of cell, confirming the system's multi-cellular targeting

Table 5
Fluorescence lifetime of RBDEC and AA in Caco-2 cells line.

Sample	τ_1 (ns)	τ_2 (ns)	τ_3 (ns)	f_1 (%)	f_2 (%)	f_3 (%)	χ^2
RBDEC	5.2 (0.1)	2.0 (0.1)	0.9 (0.1)	9 (2)	52 (2)	39 (3)	0.988–1.027
AA	2.1 (0.1)	0.8 (0.1)	–	55 (2)	45 (2)	–	1.037

capability. This strategy not only provides photodynamic efficiency but also allows for the optimization of absorbed photons. These findings encourage further investigation of dual-target systems at different concentrations and across various cancer cell lines, paving the way for the development of multifunctional DPPC/F127 vesicles with diverse photosensitizer combinations.

CRediT authorship contribution statement

Ana Claudia Pedrozo da Silva: Writing – original draft, Validation, Methodology, Investigation, Formal analysis, Data curation, Conceptualization. **Camila Fabiano de Freitas:** Writing – original draft, Methodology, Formal analysis, Conceptualization. **Italo Rodrigo Calori:** Writing – original draft, Methodology, Formal analysis. **Antonio Claudio Tedesco:** Methodology, Formal analysis. **Amanda Gratão Silvestrin:** Methodology, Formal analysis. **Leandro Herculano da Silva:** Methodology, Formal analysis, Conceptualization. **Maria Ida Bonini Ravanelli Speziali:** Writing – original draft, Methodology, Formal analysis, Conceptualization. **Noboru Hioka:** Supervision, Resources, Project administration, Funding acquisition, Conceptualization. **André Luiz Tessaro:** Writing – original draft, Supervision, Resources, Project administration, Methodology, Funding acquisition, Formal analysis, Conceptualization.

Declaration of competing interest

The authors declare the following financial interests/personal relationships which may be considered as potential competing interests: Leandro Herculano da Silva reports financial support was provided by National Council for Scientific and Technological Development. Ana Claudia Pedrozo da Silva reports financial support was provided by Coordination of Higher Education Personnel Improvement. Andre Luiz Tessaro reports financial support was provided by National Council for Scientific and Technological Development. Andre Luiz Tessaro reports financial support was provided by Federal Technological University of Paraná. If there are other authors, they declare that they have no known competing financial interests or personal relationships that could have appeared to influence the work reported in this paper.

Acknowledgments

ACPS acknowledges CAPES (Brazil) for the scholarship (n° 88887.507572/2020–00). LHS thanks CNPq (processes 200176/2024-2 and 303635/2022-3). MIBRS also acknowledges CNPq (process 408561/2023-8). ALT acknowledges UTFPR, CNPq (process 420280/2023–5) and Fundação Araucária (PRD2023361000418, PBA2025201000164) for the financial support. The authors are grateful to the National Institute of Science and Technology in Polysaccharides (INCT Polissacar- ídeos - 406973/2022-9), and Institute for Research and Innovation in Photothermal Imaging (INPIIF - 408454/ 2024-5). We are also grateful to the multiuser laboratory LAMAP/UTFPR, the Foundation for Research and Innovation Support of the State of Santa Catarina (FAPESC), and the Complex of Research Support Centers (Comcap/UEM) for their support.

Appendix A. Supplementary data

Supplementary data to this article can be found online at https://doi.org/10.1016/j.jddst.2026.108018.

Data availability

No data was used for the research described in the article.

References

[1] C.F. Cuadrado, K.J. Lagos, M.D. Stringasci, V.S. Bagnato, M.P. Romero, Clinical and pre-clinical advances in the PDT/PTT strategy for diagnosis and treatment of cancer, Photodiagnosis Photodyn. Ther. 50 (2024) 104387, https://doi.org/10.1016/j.pdpdt.2024.104387.
[2] H. Kirla, J. Wu, J. Hamzah, D.J. Henry, One-pot synthesis and covalent conjugation of methylene blue in mesoporous silica nanoparticles – a platform for enhanced photodynamic therapy, Colloids Surf. B Biointerfaces 245 (2025) 114195, https://doi.org/10.1016/j.colsurfb.2024.114195.
[3] D. Aebisher, S. Czech, K. Dynarowicz, M. Misiołek, K. Komosińska-Vassev, A. Kawczyk-Krupka, D. Bartusik-Aebisher, Photodynamic therapy: past, current, and future, Indian J. Manag. Sci. 25 (2024) 11325, https://doi.org/10.3390/ijms252011325.
[4] T.E. Kim, J.-E. Chang, Recent studies in photodynamic therapy for cancer treatment: from basic research to clinical trials, Pharmaceutics 15 (2023) 2257, https://doi.org/10.3390/pharmaceutics15092257.
[5] A.P. Castano, T.N. Demidova, M.R. Hamblin, Mechanisms in photodynamic therapy: part one—photosensitizers, photochemistry and cellular localization, Photodiagnosis Photodyn. Ther. 1 (2004) 279–293, https://doi.org/10.1016/S1572-1000(05)00007-4.
[6] M. Molica, S. Perrone, C. Mazzone, L. Cesini, M. Canichella, P. De Fabritiis, CPX-351: an old scheme with a new formulation in the treatment of high-risk AML, Cancers 14 (2022) 2843, https://doi.org/10.3390/cancers14122843.
[7] S. Alotaibi, D. Niederwieser, S.O. Ahmed, J. Sanz, M. Mohty, M. Aljurf, Current status of CPX-351 therapy in acute Myeloid leukemia and myelodysplastic syndrome, Clin. Lymphoma Myeloma Leuk. 22 (2022) 575–580, https://doi.org/10.1016/j.clml.2022.02.008.
[8] M. Mušković, R. Pokrajac, N. Malatesti, Combination of two photosensitisers in anticancer, antimicrobial and upconversion photodynamic therapy, Pharmaceuticals 16 (2023) 613, https://doi.org/10.3390/ph16040613.
[9] P. Acedo, J.C. Stockert, M. Cañete, A. Villanueva, Two combined photosensitizers: a goal for more effective photodynamic therapy of cancer, Cell Death Dis. 5 (2014) e1122, https://doi.org/10.1038/cddis.2014.77.
[10] A. Villanueva, J.C. Stockert, M. Cañete, P. Acedo, A new protocol in photodynamic therapy: enhanced tumour cell death by combining two different photosensitizers, Photochem. Photobiol. Sci. 9 (2010) 295–297, https://doi.org/10.1039/b9pp00153k.
[11] E.B. Gyenge, D. Lüscher, P. Forny, M. Antoniol, G. Geisberger, H. Walt, G. Patzke, C. Maake, Photodynamic mechanisms induced by a combination of hypericin and a chlorin based-photosensitizer in head and neck squamous cell carcinoma cells, Photochem. Photobiol. 89 (2013) 150–162, https://doi.org/10.1111/j.1751-1097.2012.01217.x.
[12] X. Schneider-Yin, A. Kurmanaviciene, M. Roth, M. Roos, A. Fedier, E.I. Minder, H. Walt, Hypericin and 5-aminolevulinic acid-induced protoporphyrin IX induce enhanced phototoxicity in human endometrial cancer cells with non-coherent white light, Photodiagnosis Photodyn. Ther. 6 (2009) 12–18, https://doi.org/10.1016/j.pdpdt.2009.02.001.
[13] S. Cao, Y. Liu, X. Tai, L. Shen, H. Yang, F. Li, B. Sui, P. Ma, L. Zhu, B. Gao, A. Wang, M. Azam, A dual-type I/II NIR photosensitizer for effective cancer photodynamic therapy with enhanced ROS generation, RSC Adv. 15 (2025) 28889–28896, https://doi.org/10.1039/D5RA05267J.
[14] A.C. Pedrozo Da Silva, C. Fabiano De Freitas, R.H. Saatkamp, E.V. Bergmann, W. Caetano, L.C. Malacarne, R.B. Samulewski, F.A. Pereira Scacchetti, N. Hioka, A. L. Tessaro, Liposomal rose bengal and its butyl ester derivative formulations for antimicrobial photodynamic therapy, J. Drug Deliv. Sci. Technol. 100 (2024) 106085, https://doi.org/10.1016/j.jddst.2024.106085.
[15] K.R. Kasimova, M. Sadasivam, G. Landi, T. Sarna, M.R. Hamblin, Potentiation of photoinactivation of Gram-positive and Gram-negative bacteria mediated by six phenothiazinium dyes by addition of azide ion, Photochem. Photobiol. Sci. 13 (2014) 1541–1548, https://doi.org/10.1039/c4pp00021h.
[16] P.C. de S. Pereira, P.F. do A. Costa, D.S. Pellosi, I.R. Calori, B.H. Vilsinski, B. M. Estevão, N. Hioka, W. Caetano, Photophysical properties and interaction studies of rose bengal derivatives with biomimetic systems based in micellar aqueous solutions, J. Mol. Liq. 230 (2017) 674–685, https://doi.org/10.1016/j.molliq.2017.01.055.
[17] C.F. de Freitas, I.R. Calori, A.C.P. da Silva, L.V. de Castro, F. Sato, D. Silva Pellosi, A.L. Tessaro, W. Caetano, N. Hioka, PEG-coated vesicles from Pluronic/lipid mixtures for the carrying of photoactive erythrosine derivatives, Colloids Surf. B Biointerfaces 175 (2019) 530–544, https://doi.org/10.1016/j.colsurfb.2018.12.031.

[18] G. Braga, K. da S.S. Campanholi, S.B. de S. Ferreira, I.R. Calori, J.H. de Oliveira, D. Vanzin, M.L. Bruschi, R.M. Pontes, P.H. Março, A.L. Tessaro, N. Hioka, W. Caetano, Tautomeric and aggregational dynamics of curcumin-supersaturated pluronic nanocarriers, ACS Appl. Polym. Mater. 2 (2020) 4493–4511, https://doi.org/10.1021/acsapm.0c00589.
[19] J.R. Lakowicz, B.R. Masters, Principles of Fluorescence Spectroscopy, third ed., 2008 029901, https://doi.org/10.1117/1.2904580. J. Biomed. Opt. 13.
[20] B.R. Rabello, A.P. Gerola, D.S. Pellosi, A.L. Tessaro, J.L. Aparício, W. Caetano, N. Hioka, Singlet oxygen dosimetry using uric acid as a chemical probe: systematic evaluation, J. Photochem. Photobiol. Chem. 238 (2012) 53–62, https://doi.org/10.1016/j.jphotochem.2012.04.012.
[21] B. Dhaini, L. Wagner, M. Moinard, J. Daouk, P. Arnoux, H. Schohn, P. Schneller, S. Acherar, T. Hamieh, C. Frochot, Importance of Rose bengal loaded with nanoparticles for anti-cancer photodynamic therapy, Pharmaceuticals 15 (2022) 1093, https://doi.org/10.3390/ph15091093.
[22] T. Entradas, S. Waldron, M. Volk, The detection sensitivity of commonly used singlet oxygen probes in aqueous environments, J. Photochem. Photobiol. B Biol. 204 (2020) 111787, https://doi.org/10.1016/j.jphotobiol.2020.111787.
[23] J.A. Bonacin, F.M. Engelmann, D. Severino, H.E. Toma, M.S. Baptista, Singlet oxygen quantum yields (Φd) in water using beetroot extract and an array of LEDs, J. Braz. Chem. Soc. 20 (2009) 31–36, https://doi.org/10.1590/S0103-50532009000100006.
[24] T.-C. Chou, Drug combination studies and their synergy quantification using the chou-talalay method, Cancer Res. 70 (2010) 440–446, https://doi.org/10.1158/0008-5472.CAN-09-1947.
[25] T.-C. Chou, Theoretical basis, experimental design, and computerized simulation of synergism and antagonism in drug combination studies, Pharmacol. Rev. 58 (2006) 621–681, https://doi.org/10.1124/pr.58.3.10.
[26] M. Danaei, M. Dehghankhold, S. Ataei, F. Hasanzadeh Davarani, R. Javanmard, A. Dokhani, S. Khorasani, M. Mozafari, Impact of particle size and polydispersity index on the clinical applications of lipidic nanocarrier systems, Pharmaceutics 10 (2018) 57, https://doi.org/10.3390/pharmaceutics10020057.
[27] D.C.S. de Oliveira, C.F. de Freitas, I.R. Calori, R.S. Goncalves, C.A.E.F. Cardinali, L. C. Malacarne, M.I. Ravanelli, H.P.M. de Oliveira, A.C. Tedesco, W. Caetano, N. Hioka, A.L. Tessaro, Theranostic verteporfin- loaded lipid-polymer liposome for photodynamic applications, J. Photochem. Photobiol. B Biol. 212 (2020) 112039, https://doi.org/10.1016/j.jphotobiol.2020.112039.
[28] S. Bibi, R. Kaur, M. Henriksen-Lacey, S.E. McNeil, J. Wilkhu, E. Lattmann, D. Christensen, A.R. Mohammed, Y. Perrie, Microscopy imaging of liposomes: from coverslips to environmental SEM, Int. J. Pharm. 417 (2011) 138–150, https://doi.org/10.1016/j.ijpharm.2010.12.021.
[29] Y. Talmon, Staining and drying-induced artifacts in electron microscopy of surfactant dispersions, J. Colloid Interface Sci. 93 (1983) 366–382, https://doi.org/10.1016/0021-9797(83)90420-4.
[30] A.C.P. da Silva, D. Vanzin, D.L.M. Tolari, W. Caetano, R.M. Pontes, P.H. Março, N. Hioka, R.B. Samulewski, A.C. Gracetto, A.L. Tessaro, Application of chemometric method and computational analysis in the spectroscopic study of azure A dimerization, J. Mol. Liq. 366 (2022) 120316, https://doi.org/10.1016/j.molliq.2022.120316.
[31] T.M. Allen, P.R. Cullis, Liposomal drug delivery systems: from concept to clinical applications, Adv. Drug Deliv. Rev. 65 (2013) 36–48, https://doi.org/10.1016/j.addr.2012.09.037.
[32] J.R. Lakowicz, S. Keating-Nakamoto, Red-edge excitation of fluorescence and dynamic properties of proteins and membranes, Biochemistry 23 (1984) 3013–3021, https://doi.org/10.1021/bi00308a026.
[33] S.K. Cushing, M. Li, F. Huang, N. Wu, Origin of strong excitation wavelength dependent fluorescence of graphene oxide, ACS Nano 8 (2014) 1002–1013, https://doi.org/10.1021/nn405843d.
[34] J. Fang, H. Nakamura, H. Maeda, The EPR effect: unique features of tumor blood vessels for drug delivery, factors involved, and limitations and augmentation of the effect, Adv. Drug Deliv. Rev. 63 (2011) 136–151, https://doi.org/10.1016/j.addr.2010.04.009.
[35] C. Demetzos, Differential Scanning calorimetry (DSC): a tool to study the thermal behavior of lipid bilayers and liposomal stability, J. Liposome Res. 18 (2008) 159–173, https://doi.org/10.1080/08982100802310261.
[36] G. Neunert, J. Tomaszewska-Gras, A. Baj, M. Gauza-Włodarczyk, S. Witkowski, K. Polewski, Phase transitions and structural changes in DPPC liposomes induced by a 1-Carba-Alpha-Tocopherol analogue, Molecules 26 (2021) 2851, https://doi.org/10.3390/molecules26102851.
[37] Y. Liu, L. Si, Y. Jiang, S. Jiang, X. Zhang, S. Li, J. Chen, J. Hu, Design of pH-Responsive nanomaterials based on the tumor microenvironment, IJN 20 (2025) 705–721, https://doi.org/10.2147/IJN.S504629.
[38] I.R. Calori, D.S. Pellosi, D. Vanzin, G.B. Cesar, P.C.S. Pereira, M.J. Politi, N. Hioka, W. Caetano, Distribution of xanthene dyes in DPPC vesicles: rationally accounting for drug partitioning using a membrane model, J. Braz. Chem. Soc. 27 (2016) 1938–1948, https://doi.org/10.5935/0103-5053.20160079.
[39] J. Repáková, P. Čapková, J.M. Holopainen, I. Vattulainen, Distribution, orientation, and dynamics of DPH probes in DPPC bilayer, J. Phys. Chem. B 108 (2004) 13438–13448, https://doi.org/10.1021/jp048381g.
[40] J. Repáková, J.M. Holopainen, M.R. Morrow, M.C. McDonald, P. Čapková, I. Vattulainen, Influence of DPH on the structure and dynamics of a DPPC bilayer, Biophys. J. 88 (2005) 3398–3410, https://doi.org/10.1529/biophysj.104.055533.
[41] S.S. Arumugam, N. Subramanian, I. Malaichamy, New insights into the dimerization and site-specific cooperative interaction of Azure B with model transport proteins by spectroscopic and computational studies, J. Photochem. Photobiol. B Biol. 164 (2016) 212–225, https://doi.org/10.1016/j.jphotobiol.2016.09.011.
[42] A. Raudino, F. Guerrera, A. Asero, V. Rizza, Application of red-edge effect on the mobility of membrane lipid polar head groups, FEBS (Fed. Eur. Biochem. Soc.) Lett. 159 (1983) 43–46, https://doi.org/10.1016/0014-5793(83)80413-X.
[43] A. Chattopadhyay, S. Mukherjee, Red edge excitation shift of a deeply embedded membrane probe: implications in water penetration in the bilayer, J. Phys. Chem. B 103 (1999) 8180–8185, https://doi.org/10.1021/jp991303m.
[44] L. M, J. P, A. Paula, D. Severino, M. Regina, H.P.M. de Oliveir, Phenotiazinium dyes as photosensitizers (PS) in photodynamic therapy (PDT): spectroscopic properties and photochemical mechanisms, in: M. Akhyar Farrukh (Ed.), Advanced Aspects of Spectroscopy, InTech, 2012, https://doi.org/10.5772/48087.
[45] X. Li, M. Wang, Y. Yang, B. Lei, S. Ma, Y. Yu, Influence of nutrients on the bioaccessibility and transepithelial transport of polybrominated diphenyl ethers measured using an in vitro method and Caco-2 cell monolayers, Ecotoxicol. Environ. Saf. 208 (2021) 111569, https://doi.org/10.1016/j.ecoenv.2020.111569.
[46] M. Wainwright, The development of phenothiazinium photosensitisers, Photodiagnosis Photodyn. Ther. 2 (2005) 263–272, https://doi.org/10.1016/S1572-1000(05)00110-9.
[47] P.-T. Wu, C.-L. Lin, C.-W. Lin, N.-C. Chang, W.-B. Tsai, J. Yu, Methylene-blue-encapsulated liposomes as photodynamic therapy nano agents for breast cancer cells, Nanomaterials 9 (2018) 14, https://doi.org/10.3390/nano9010014.
[48] E.M. Klosowski, B.T.L. De Souza, M.S. Mito, R.P. Constantin, G.C. Mantovanelli, J. M. Mewes, P.F.V. Bizerra, P.V.M.D.C. Menezes, E.H. Gilglioni, K.S. Utsunomiya, R. Marchiosi, W.D. Dos Santos, O.F. Filho, W. Caetano, P.C.D.S. Pereira, R. S. Gonçalves, J. Constantin, E.L. Ishii-Iwamoto, R.P. Constantin, The photodynamic and direct actions of methylene blue on mitochondrial energy metabolism: a balance of the useful and harmful effects of this photosensitizer, Free Radic. Biol. Med. 153 (2020) 34–53, https://doi.org/10.1016/j.freeradbiomed.2020.04.015.
[49] E.M. Klosowski, B.T.L. De Souza, L.F. Nanami, M.C. Da Silva, M.S. Mito, G.N. M. Esquissato, B.M. Joia, P.V.M.D.C. Menezes, W. Caetano, P.C.D.S. Pereira, J. J. Dos Santos, R.B. Balbinot, F.P. Garcia, D.L. Bidoia, T.U. Nakamura, C. V. Nakamura, E.L. Ishii-Iwamoto, A.P. Ferro, W.D. Dos Santos, O. Ferrarese-Filho, R. Marchiosi, R.P. Constantin, Beyond phototoxicity: the dark side of new methylene blue on mitochondrial and cellular bioenergetics, Free Radic. Biol. Med. 240 (2025) 314–338, https://doi.org/10.1016/j.freeradbiomed.2025.08.037.
[50] L.D. Mayer, T.O. Harasym, P.G. Tardi, N.L. Harasym, C.R. Shew, S.A. Johnstone, E. C. Ramsay, M.B. Bally, A.S. Janoff, Ratiometric dosing of anticancer drug combinations: controlling drug ratios after systemic administration regulates therapeutic activity in tumor-bearing mice, Mol. Cancer Therapeut. 5 (2006) 1854–1863, https://doi.org/10.1158/1535-7163.MCT-06-0118.
[51] T.-C. Chou, P. Talalay, Quantitative analysis of dose-effect relationships: the combined effects of multiple drugs or enzyme inhibitors, Adv. Enzym. Regul. 22 (1984) 27–55, https://doi.org/10.1016/0065-2571(84)90007-4.
[52] Z.-G. Yue, W. Wei, P.-P. Lv, H. Yue, L.-Y. Wang, Z.-G. Su, G.-H. Ma, Surface charge affects cellular uptake and intracellular trafficking of chitosan-based nanoparticles, Biomacromolecules 12 (2011) 2440–2446, https://doi.org/10.1021/bm101482r.
[53] Z. Yu, W. Pan, N. Li, B. Tang, A nuclear targeted dual-photosensitizer for drug-resistant cancer therapy with NIR activated multiple ROS, Chem. Sci. 7 (2016) 4237–4244, https://doi.org/10.1039/C6SC00737F.
[54] I.R. Calori, W. Caetano, A.C. Tedesco, N. Hioka, Self-aggregation of verteporfin in glioblastoma multiforme cells: a static and time-resolved fluorescence study, Dyes Pigments 182 (2020) 108598, https://doi.org/10.1016/j.dyepig.2020.108598.
[55] J.P. Tardivo, A. Del Giglio, C.S. de Oliveira, D.S. Gabrielli, H.C. Junqueira, D. B. Tada, D. Severino, R. de Fátima Turchiello, M.S. Baptista, Methylene blue in photodynamic therapy: from basic mechanisms to clinical applications, Photodiagnosis Photodyn. Ther. 2 (2005) 175–191, https://doi.org/10.1016/S1572-1000(05)00097-9.
[56] T.M. Tsubone, W.K. Martins, C. Pavani, H.C. Junqueira, R. Itri, M.S. Baptista, Enhanced efficiency of cell death by lysosome-specific photodamage, Sci. Rep. 7 (2017) 6734, https://doi.org/10.1038/s41598-017-06788-7.
[57] A.A. Salim, S.K. Ghoshal, M.S. Shamsudin, M.I. Rosli, M.S. Aziz, S.W. Harun, G. Krishnan, H. Bakhtiar, Absorption, fluorescence and sensing quality of Rose Bengal dye-encapsulated cinnamon nanoparticles, Sensor Actuator Phys. 332 (2021) 113055, https://doi.org/10.1016/j.sna.2021.113055.
[58] I.R. Calori, A.C. Tedesco, Aluminum chloride phthalocyanine in MCF-7: rationally accounting for state of aggregation of photosensitizers inside cells, Dyes Pigments 173 (2020) 107940, https://doi.org/10.1016/j.dyepig.2019.107940.
[59] C.C. Jayme, I.R. Calori, E.M.F. Cunha, A.C. Tedesco, Evaluation of aluminum phthalocyanine chloride and DNA interactions for the design of an advanced drug delivery system in photodynamic therapy, Spectrochim. Acta Mol. Biomol. Spectrosc. 201 (2018) 242–248, https://doi.org/10.1016/j.saa.2018.05.009.